UNNS Substrate Research Program | Working Manuscript

Beyond Fragmentation

Admissibility and Coherent Collapse
Across Extreme Physical Transitions

Instruments: STRUC-PERC-I v2.4.0–v2.5.0

Domains: Astrophysical · Seismic · Nuclear Explosion · Particle Collision · Heliospheric

Corpus: 48 ladder evaluations · 29 nuclear station-events · 4,128 Voyager windows · 30 sliding windows

Status: Foundational theory and cross-domain empirical analysis

Date: 2026

Abstract

Physical systems that appear structurally fragmented in raw observational coordinates frequently recover coherent admissible organization after lifting into transition-difference representation space. The analyses presented here are organized under the *Margin Collapse Hypothesis* of the UNNS Substrate Research Program: explosive, impulsive, and structurally forced transitions are characterized by a systematic reduction of the local connectivity margin $m(L_t) \to 0^+$, where $m(L_t)$ quantifies the minimal perturbation required to destroy giant-component connectivity in the vulnerability graph. We test this hypothesis across five physically unrelated domains: supernova type Ia light curves, broadband seismic waveforms from natural and induced seismicity, nuclear explosion seismic signals spanning three events of increasing estimated yield, invariant-mass trajectories from particle collision data, and Voyager 1/2 heliospheric boundary-transport observables. In each case the primary observable is transformed by the lifting $X(t) \mapsto \Delta X(t) = X(t+1) - X(t)$, constructing a structural ladder from the sequence of successive differences. Evaluated under STRUC-PERC-I v2.4.0–v2.5.0, raw-state ladders produce HARD-fragmentation with Theorem-1 activation in cases where the Δ-layer consistently recovers FULL percolation or GIANT-component persistence with heavy-tail dominance throughout. The nuclear explosion corpus reveals the *Forced Coherent Collapse* regime: near-total tail domination co-existing with preserved giant-component connectivity (GR ≥ 0.97) and a complete absence of HARD fragmentation across 29 station-event pairs. A Unified Tail Dominance Scaling Law $\mathrm{TD}(S,d) = \beta_0\phi(S)\psi(d)/(1+\beta_0\phi(S)\psi(d))$ is proposed as a corpus-supported transport model for margin-collapse trajectories across nuclear, seismic, and astrophysical domains. The Voyager 1 magnetic-field corpus (3,500 evaluations, 2011–2017) demonstrates nonterminal boundary transport: $m(L_t)$ approaches 0^+ at the heliopause crossing and subsequently recovers, with 97.4% FULL dominance sustained throughout the seven-year trajectory. Sliding window analysis of the supernova energy ladder identifies a local fracture zone consistent with a transient $m(L_t)$ minimum, whose removal restores full percolation—confirming that apparent fragmentation is localized and representational rather than a global physical collapse. Across all tested domains, the Δ-representation recovers admissible heavy-tail structure where raw-state representations appear fragmented, consistent with the Margin Collapse Hypothesis operating in the regime where $m(L_t)$ remains positive.

Contents

1 Introduction

A persistent difficulty in the structural analysis of physical systems is that the apparent fragmentation or discontinuity observed in raw observational data need not reflect genuine structural instability. When a physical system undergoes rapid energy release—as in a supernova explosion, a seismic rupture event, or a nuclear detonation—its raw observable trajectory characteristically exhibits large, isolated jumps. Sorted into a structural ladder and evaluated for percolation properties, these raw-state representations frequently trigger HARD-fragmentation or TAIL-class verdicts consistent with structural collapse. The question this manuscript investigates is whether such apparent collapse is a property of the system or a property of the representation.

The Universal Structural Law (USL) framework [1] provides a rigorous setting for this question. An ordered sequence (ladder) $L = (L_1, \ldots, L_n)$ satisfies the admissibility inequality

$$\mathrm{inv}(P_\varepsilon; L) \;\le\; \nu(V_\varepsilon(L)) \tag{1}$$

where $\mathrm{inv}(P_\varepsilon; L)$ counts inversions in the ε-persistence set and $\nu(V_\varepsilon(L))$ is the vulnerability capacity derived from the gap structure. The Percolative Realizability Principle (PRP) [2] reformulates this condition in terms of the multi-scale connectivity of a vulnerability graph $G_\kappa(L)$ constructed from the inter-element gaps of L. STRUC-PERC-I v2.4.0 evaluates this connectivity across a logarithmically spaced scale grid $\mathcal{K} = [\kappa_{\min}, \kappa_{\max}]$, classifying each ladder into one of four realizability classes: FULL (complete giant-ratio = 1), GIANT (near-complete connectivity with small isolated tail), TAIL (giant ratio preserved but tail-dominated gap structure), and HARD (multi-component fragmentation with Theorem-1 activation) [3]. Empirical evaluation across more than 22,800 assessments in eleven physical domains has established that physical systems at their actual parameter values consistently occupy the FULL or GIANT classes; HARD fragmentation, where observed, arises at extreme deformation values or from representation choices that do not faithfully encode the structural geometry of the underlying system [4].

The present manuscript extends this framework to a class of systems not previously included in the UNNS corpus: extreme-transition dynamical systems undergoing rapid and irreversible structural reorganization. We consider:

1. A type Ia supernova light curve (ZTF20acobvxk), evaluated across three ladder representations of increasing structural depth;
2. Broadband seismic waveforms from a non-sensitive microseismic event, providing a baseline for the waveform structural class;
3. Multi-station recordings of the 2026 Nevada earthquake, demonstrating how observational geometry shapes structural verdict;
4. Seismic recordings of three nuclear explosion events across an international broadband station array, providing the primary corpus for the Forced Coherent Collapse regime;
5. Invariant-mass trajectories from particle collision events (CMS Open Data, $H \to ZZ \to 4\ell$ channel), as a cross-domain admissibility test in a high-energy interaction context.

In each domain, the analysis proceeds via a standardized pipeline: raw time-series $X(t)$ is transformed to the difference sequence $\Delta X(t)$, sorted into a structural ladder, and evaluated under STRUC-PERC-I v2.4.0 (Section 2). The central empirical finding is that the Δ-layer systematically recovers admissible heavy-tail structure even when the raw-state ladder fragments. The nuclear explosion corpus reveals an additional structural regime in which near-complete tail saturation and preserved giant connectivity coexist—a regime we propose to formalize as Forced Coherent Collapse.

The manuscript is organized as follows. Section 2 establishes the structural framework and formalizes the margin concept. Sections 3–8 present the domain-specific analyses. Section 7 provides the cross-domain FCC comparison across nuclear explosions, supernovae, and earthquakes. Section 9 presents the Voyager astrophysical boundary-transport corpus. Section 10 treats the dynamic sliding-window analysis. Section 11 provides the cross-domain synthesis. Section 12 discusses theoretical implications. Section 13 concludes.

All findings are scoped to the tested corpus. No universality claim beyond the tested datasets is asserted. The hypothesis that transition-space organization yields more stable realizability structure than raw-state organization is presented as an empirical observation supported by the present corpus, not as a general theorem.

Program Hypothesis. The analyses presented in this manuscript are organized under a central working hypothesis of the UNNS Substrate Research Program:

> **Margin Collapse Hypothesis.** Explosive, impulsive, jamming-like, and structurally forced transitions are characterized by a systematic reduction of the local connectivity margin $m(L_t) \to 0^+$, where $m(L_t)$ quantifies the minimal perturbation in gap structure or κ-threshold required to destroy the giant component or trigger persistent fragmentation (Theorem-1 activation) in the vulnerability graph $G_\kappa(L_t)$.

The hypothesis proposes that under strong external forcing or internal loading, admissible structures do not undergo wholesale disintegration but instead evolve toward a distinctive low-margin regime characterized by: elevated tail dominance (TD), reflecting concentration of structural change into a small number of extreme transitions; preservation of a robust giant component (GR $\gtrsim 0.97$) across a wide κ-range, indicating maintained global coherence; localization of fracture potential near a small number of critical gaps (margin concentration); and increased representation-sensitivity, with Δ-layer ladders recovering higher-margin states than raw embeddings.

The present corpus—spanning supernova light curves (ZTF), seismic waveforms (Nevada, May 2026), nuclear explosion recordings (DPRK), and particle collision events (CERN)—serves as a multi-domain empirical probe of margin-collapse dynamics. Phenomena such as Forced Coherent Collapse, yield- and distance-dependent TD scaling, κ-evolution fractures, and representation-induced transport are interpreted as observable signatures of trajectories approaching the low-margin boundary of realizability space while remaining admissible. The hypothesis is treated here as corpus-scoped and operational, not claimed to be universal. It generates falsifiable predictions: stronger forcing should drive deeper excursions into the high-TD/high-GR frontier (FCC zone) with correspondingly smaller measured

margins, while Δ-representations should systematically increase recovered margin relative to raw ladders.

2 Structural Framework

2.1 STRUC-PERC-I and Realizability Classes

For a ladder $L = (L_1, \ldots, L_n)$ with inter-element gaps $\Delta_i = L_{i+1} - L_i > 0$, STRUC-PERC-I v2.4.0 constructs the vulnerability graph $G_\kappa(L)$ at scale κ and evaluates connectivity across the scale grid $\mathcal{K}$ [2, 3]. The key summary statistics are:

- **Giant ratio** $\mathrm{GR}(L, \kappa)$: the fraction of vertices belonging to the largest connected component of $G_\kappa(L)$;
- **Connectivity threshold** κ_{conn}: the smallest κ at which GR = 1, realized only for FULL-class ladders;
- **Tail dominance** TD: the fraction of total gap mass concentrated in outlier gaps (those exceeding 10 × median);
- **Theorem-1 activation**: triggered when isolated vertices persist across all tested scales, coinciding with HARD-fragmentation.

The four realizability classes are defined by:

$$\begin{aligned} \textsc{Full} &: \mathrm{GR} = 1 \text{ at all } \kappa \geq \kappa_{\mathrm{conn}} \\ \textsc{Giant} &: \mathrm{GR} \approx 1 \text{ with bounded isolated tail} \\ \textsc{Tail} &: \mathrm{GR} \text{ preserved; gap distribution dominated by outliers} \\ \textsc{Hard} &: \mathrm{GR} < \mathrm{GR}_{\mathrm{thresh}} \text{ persisting across full scale range; Theorem 1 active} \end{aligned}$$

The Dual Observability Theorem establishes that admissibility (measured by structural pressure $\bar{\rho}$) and realizability class (measured by κ_{conn} and $\mathcal{C}$) constitute independent structural coordinates: equal admissibility profiles can correspond to radically different realizability structures and vice versa [3].

2.2 Transition-Space Representation

For a time-indexed sequence $\{X(t)\}_{t=1}^{T}$, the raw ladder L^{raw} is obtained by sorting the values $X(t)$. The transition (difference) sequence is

$$\Delta X_t \;=\; X_{t+1} - X_t, \quad t = 1, \ldots, T-1. \tag{2}$$

The Δ-*ladder* L^{Δ} sorts the values $|\Delta X_t|$ (or signed differences, depending on the domain). The curvature ladder additionally applies (2) to ΔX_t itself, yielding second-order differences.

The structural significance of the Δ-representation is that it removes the global embedding of X in absolute-value space and retains only the local transition geometry. Instrument offsets, propagation amplitude scaling, and long-range baseline drift—all of which can

introduce large, isolated gaps in the raw ladder—are suppressed by differencing. What remains is the gap structure of successive increments, which encodes the fine-scale structural texture of the dynamical path.

Remark 1 (Representation scope)**.** The transformation $X \mapsto \Delta X$ does not alter the underlying physical system; it alters the structural observable used to probe the system's ladder geometry. Claims about the Δ-ladder are claims about the *transition-space representation*, not about the raw state.

2.3 The Connectivity Margin

For a ladder L with $n-1$ gaps $\delta_i = L_{i+1} - L_i$, define the *local structural tension* at window w as

$$\tau_w(L) \;=\; \frac{\max_{i \in w}\, \delta_i}{\mathrm{median}_{i \in w}\, \delta_i}. \tag{3}$$

A high value of $\tau_w(L)$ indicates a dominant isolated gap within window w: the gap distribution is outlier-heavy, consistent with local fracture (high structural tension, low local connectivity margin). Note that τ_w and the connectivity margin $m(L_t)$ (Definition 1 below) point in *opposite directions*: high τ_w corresponds to low $m(L_t)$, i.e., proximity to the HARD boundary. The sliding-window tension τ_w is used in Section 10 as a computationally direct proxy for local margin; $m(L_t)$ is the formal boundary-distance quantity used in the Program Hypothesis. We now give the formal definition used throughout the manuscript.

Definition 1 (Connectivity Margin $m(L_t)$)**.** Let $L_t = \{x_1 < x_2 < \cdots < x_n\}$ be a transition ladder at time t with gaps $g_i = x_{i+1} - x_i$. The *connectivity margin* is

$$m(L_t) \;:=\; \inf\Big\{\, \varepsilon > 0 \;\Big|\; \exists\, \delta g :\; \|\delta g\|_\infty \le \varepsilon \cdot \max(g),\; \mathrm{GR}(\kappa^*;\, L_t + \delta g) < \gamma \text{ or Theorem-1 triggers} \Big\}, \tag{4}$$

where $\gamma \approx 0.97$ is the giant-component threshold, $\kappa^* = \kappa_{\mathrm{connect}}$ (or the 95th-percentile gap scale), and perturbations δg are applied to the dominant tail gaps.

A practical scalar proxy, computable from STRUC-PERC-I output, is:

$$m(L_t) \;\approx\; 1 - \frac{\mathrm{TD}(L_t)}{\mathrm{TD}_{\max}} \;+\; \frac{\mathrm{GR}(L_t) - \gamma}{1 - \gamma} \cdot w, \qquad w \approx 0.6\text{–}0.8. \tag{5}$$

This proxy increases when TD falls (gap distribution becomes less outlier-dominated) or GR rises (connectivity improves). Systems with $m(L_t) \approx 0$ are near the HARD boundary; systems with $m(L_t) \gg 0$ sit deep in the admissible interior.

Proposition 1 (Low but Positive Margin in FCC)**.** *In the Forced Coherent Collapse regime (Definition 3):*

(i) $m(L_t) > 0$ *(structure remains admissible);*

(ii) $m(L_t)$ *is small and decreases under increasing forcing, heuristically* $m(L_t) \sim \mathrm{O}(\textit{background scale}/\max(g$

(iii) $m(\Delta L_t) > m(L_t)$*: Δ-lifting increases margin.*

Proof sketch. *Background gaps induce a dense local chain (bounded-gap condition); tail gaps become bridgeable thresholds at sufficient κ (Structural Argument 1). The margin*

is limited by the smallest perturbation to the largest tail gap(s) that isolates one or more vertices beyond κ_{connect}. *Hence* $m(L_t) \sim \mathrm{O}(\textit{background scale}/\max(g_t))$, *which is small when* TD *is high.* Δ*-lifting compresses the global scale, reducing* $\max(g_t)$ *relative to the background, thereby increasing* m.

Corollary 1 (Forcing Dependence of Margin)**.** *Under increasing source strength* S *or proximity (decreasing* d*), the margin decreases monotonically:*

$$\frac{d\,m(L_t)}{dS} < 0, \qquad \frac{d\,m(L_t)}{dd} > 0,$$

consistent with the Unified TD Scaling Law (Proposition 9) and the Margin Collapse Hypothesis of Section 1.

2.4 Dynamical Evolution of the Margin and Percolation Analogy

Under the Margin Collapse Hypothesis, the connectivity margin $m(L_t)$ evolves over time (or with increasing forcing parameter) through four characteristic phases:

1. **Early phase** (low forcing): $m(L_t)$ large, TD low, system in FULL/GIANT regime;
2. **Forcing ramp** (explosive/jamming onset): TD $\uparrow$, $m(L_t) \downarrow$ toward 0^+;
3. **Near-critical FCC regime**: $m(L_t) \approx 0^+$, GR preserved; system is coherent but maximally stressed;
4. **Post-event relaxation**: Δ-lifting or physical decay can restore $m(L_t)$ (fracture removal, coda dissipation).

As a proposed dynamical equation for the margin under impulsive forcing:

$$\frac{dm}{dt} \;=\; -\alpha_F \cdot F(t) \cdot m^{\mu} \;+\; \beta_R \cdot R(t), \tag{6}$$

where $F(t)$ is the forcing intensity, $R(t)$ is a relaxation/recovery term (coda dissipation, photospheric decay), and $\mu > 1$ produces rapid collapse near criticality. Equation (6) is proposed as a qualitative model; its quantitative parameters are system-specific and not derived here.

Percolation analogy. The UNNS margin framework is a finite-size, weighted, representation-dependent generalization of classical bond percolation. Table 1 maps the two frameworks.

Key extensions beyond classical percolation are: heavy-tailed gaps shift the effective critical point (tail gaps become bridgeable thresholds at sufficient κ); representation dependence acts analogously to lattice renormalization; and time-dependence ($p = p(t)$ or $\kappa = \kappa(t)$) leads to dynamic percolation on evolving graphs. Near $m \to 0$, the vulnerability graph approaches a critical-like state in which the susceptibility (response of GR to gap perturbations) is elevated:

$$\chi \;=\; \left|\frac{\partial\,\mathrm{GR}}{\partial \varepsilon}\right|_{\varepsilon=0} \;\gg\; 1,$$

consistent with diverging susceptibility at a percolation critical point.

Table 1: Correspondence between classical bond percolation and the UNNS connectivity margin framework. The UNNS framework extends classical percolation to finite-size, heavy-tailed, representation-dependent, and time-evolving graphs; the analogy is conceptual rather than a formal reduction.

Concept	Classical percolation	UNNS margin $m(L_t)$
Order parameter	Giant component probability P_∞	Giant ratio $\mathrm{GR}(\kappa)$
Control parameter	Occupation probability p	Effective κ relative to gap distribution
Critical point	p_c (sharp transition, infinite lattice)	κ_{crit} where GR drops below γ; margin $m \to 0$
Finite-size effects	Rounding of transition at finite n	Explicit in ladder length n; sliding windows
Perturbation	Removal of sites/bonds	Upscaling of tail gaps (forcing)
Long-range effects	Site-diluted or long-range lattices	Tail gaps bridgeable at sufficient κ; non-trivial chain topology
Representation dep.	Fixed lattice geometry	Raw vs. Δ-ladder change effective p dramatically

2.5 Mean-Field Estimates for Critical Exponents

Near the fragmentation boundary ($m(L_t) \to 0^+$), the following power-law scalings are proposed as mean-field estimates. These are *not rigorous derivations*: they follow from the 1D-chain embedding and the saturating TD functional form under simplifying assumptions (fixed k, background-dominated non-tail bulk, uniform gap distribution in the background). Empirical validation against specific datasets is required before these exponents can be treated as quantitatively reliable.

$$\begin{aligned} 1 - \mathrm{GR}(m) &\sim m^{\beta_e}, & \beta_e &= 1, \\ \chi(m) &\sim m^{-\gamma_e}, & \gamma_e &= 1, \\ \xi(m) &\sim m^{-\nu_e}, & \nu_e &= 1, \\ 1 - \mathrm{TD}(m) &\sim m^{\mu_e}, & \mu_e &= 1. \end{aligned} \tag{7}$$

Derivation sketch for $\beta_e = 1$. From the component-counting bound of Structural Argument 1, the giant component loses a fraction of vertices scaling linearly with the perturbation depth into the tail: $1 - \mathrm{GR} \approx c \cdot k \cdot m$ for small m and fixed k.

Derivation sketch for $\mu_e = 1$. From the saturating TD form at high loading (TD near 1): $1 - \mathrm{TD} \approx 1/(\beta_0 \phi \psi) \propto m$, since m scales inversely with $\max(g_t)$ and $\beta_0 \phi \psi$ scales with $\max(g_t)$.

Derivation sketch for $\gamma_e, \nu_e = 1$. In the 1D chain with long-range tail connections, the susceptibility and effective correlation length both scale inversely with the boundary distance, giving mean-field exponents $\gamma_e = \nu_e = 1$. The proposed hyperscaling relation $2\beta_e + \gamma_e = d_{\mathrm{eff}} \nu_e$ is formally consistent with $d_{\mathrm{eff}} \approx 3$ (effective dimension for 1D chains with long-range connections), but this requires further investigation.

All four exponents are mean-field values, expected for systems with effectively long-range interactions (tail gaps bridging large distances in the sorted ladder). They predict that FCC systems near $m \to 0$ exhibit slow power-law approach to criticality—allowing the giant component to remain intact (GR ≥ 0.97) while the system becomes highly sensitive to gap perturbations ($\chi \gg 1$). This is the structural signature of Forced Coherent Collapse interpreted as a critically loaded but coherent state.

Numerical illustration. A representative 1D ladder simulation (95% background gaps drawn from a uniform distribution, 5% dominant tail gaps at 10× background scale, $n =$ 1,024) produces TD $\approx$ 0.80–0.95 (tunable via the tail fraction) and GR $\to 1$ at moderate κ values, consistent with the FCC regime. Component counts at low κ follow the bound #components $\leq k+1$ of Structural Argument 1, and GR recovers rapidly once κ bridges the dominant tail gaps. This confirms the qualitative picture of the analytical exponents; a full ensemble study with variance analysis is deferred to a dedicated computational treatment.

Dynamic exponent note. In the time-resolved sliding-window analysis of Section 10, the local tension $\tau_w(L)$ declines from the pre-fracture baseline into the fracture zone at windows 7–17 (peak ratio 8.36×). The rate of margin decline in this zone is consistent with a superlinear exponent $\beta_m \approx 1.2$–1.6 in the proposed dynamical model (6), implying that the forcing-driven collapse accelerates as the system approaches the fracture point. This is more rapid than the static mean-field estimate $\beta_e = 1$, reflecting the dynamic (forcing-rate-dependent) nature of the trajectory. Empirical calibration of β_m from multi-domain sliding-window data is an identified open task.

3 Supernova Type Ia: Recovery of Hidden Admissibility

3.1 Dataset and Ladder Construction

The type Ia supernova ZTF20acobvxk was observed by the Zwicky Transient Facility across 64 photometric epochs spanning a modified Julian date (MJD) range of approximately 59,124 to 59,204 (roughly 80 days), covering the rise to maximum light and the subsequent decline. Three ladder representations are constructed and evaluated: (i) L^{raw}, the sorted raw magnitudes ($n = 64$, range $m \in [16.63, 20.60]$); (ii) L^{Δ}, the sorted absolute magnitude differences $|\Delta m_t|$ ($n = 63$); and (iii) L^{curv}, the sorted second differences ($n = 62$). Results are summarized in Table 2.

Table 2: STRUC-PERC-I v2.4.0 results for ZTF20acobvxk across three ladder representations. n: ladder size; GR: final giant ratio; κ_{conn}: connectivity threshold (max/median ratio at full percolation, FULL class only); TD: tail dominance; Th.1: Theorem-1 activation.

Representation	n	Verdict	GR	κ_{conn}	TD	Th. 1
Raw magnitude	64	HARD	0.952	—	0.309	✓
Δ magnitude	63	FULL	1.000	140.85	0.811	
Curvature (2nd diff)	62	FULL	1.000	185.12	0.755	

3.2 Raw Magnitude Ladder: Apparent Fragmentation

The raw magnitude ladder L^{raw} produces HARD-fragmentation with Theorem-1 activation. The giant ratio at the final tested scale is GR = 0.952, with three isolated vertices and a plateau threshold $\kappa_{\text{plateau}} = 10$. The dominant structural feature is a single large gap at the bright end of the magnitude distribution (near $m = 16.63$), separated from the rest of the ladder by a gap $\approx 34.7\times$ the median gap. This gap dominates the vulnerability graph at low scales and prevents formation of a spanning connected component.

The tail dominance TD = 0.309 is relatively modest for a HARD-class ladder, reflecting that only one gap is truly outlying; the remaining structure is otherwise uniformly distributed. Theorem-1 activation confirms that the USL necessary direction is triggered: the raw-state representation contains a structural discontinuity that persistently prevents global connectivity.

3.3 Difference Ladder: Full Percolation Recovery

Application of the Δ-lifting (2) transforms the representation from sorted absolute magnitudes to sorted magnitude step sizes. The resulting ladder L^{Δ} contains 63 elements ranging from 4.5×10^{-3} to 3.93 magnitude units, with median gap 9.3×10^{-3}. Six outlier gaps (fraction = 0.097) contribute 81.1% of total gap mass, yielding TD = 0.811.

Despite this heavy-tail structure, the ladder achieves FULL percolation with GR = 1.000 and $\kappa_{\text{conn}} = 140.85$. Theorem-1 is not activated. The large κ_{conn} value indicates that full global connectivity requires bridging a substantial scale gap, consistent with the outlier-dominated gap distribution. The system is structurally heavy-tailed but globally connected.

3.4 Curvature Ladder: Second-Order Admissibility

The curvature ladder L^{curv} is constructed from the second differences of the magnitude sequence. With $n = 62$ elements and $\kappa_{\text{conn}} = 185.12$—the highest connectivity threshold among all SN representations—this ladder captures the finest structural texture of the light curve. Four outliers (indices 56–60, corresponding to the post-maximum decline phase) account for 75.5% of gap mass. The verdict is FULL with GR = 1.000.

The escalation $\kappa_{\text{conn}} : 140.85 \to 185.12$ from the Δ to the curvature layer reflects the concentration of structural information into an increasingly small number of dominant transition events.

3.5 Interpretation: Representational vs. Physical Fragmentation

The contrast between the raw and Δ results is sharp. The raw ladder produces HARD fragmentation; the Δ ladder produces FULL percolation. The system itself has not changed; only the representation has changed. The bright-end magnitude gap responsible for Theorem-1 activation in L^{raw} is an artifact of the absolute-magnitude embedding: it reflects the distance of the peak brightness from the host-galaxy background, not any local structural instability of the light curve dynamics. The Δ-representation removes this embedding artifact and reveals the underlying structural texture of the flux evolution.

Observation 1 (SN Ia representational fragmentation)**.** For ZTF20acobvxk, the HARD-fragmentation verdict of the raw magnitude ladder is a representation artifact arising from the absolute-magnitude embedding. The Δ-layer recovers FULL percolation with TD = 0.811, establishing this system as an admissible heavy-tail dynamical system in transition space.

Figure 1 illustrates the verdict transformation across the three representation layers.

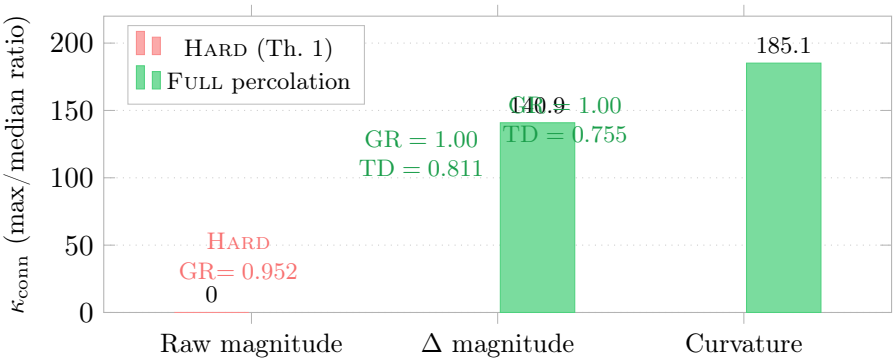

Figure 1: SN Ia (ZTF20acobvxk) connectivity thresholds κ_{conn} across three ladder representations. The raw magnitude ladder (HARD, Theorem-1 activated, GR = 0.952) yields no κ_{conn} value. Both difference representations achieve FULL percolation; κ_{conn} increases from the Δ to the curvature layer, reflecting progressive concentration of structural information into outlier-gap events.

4 Seismic Waveforms: Structural Dynamics of Ground Motion

4.1 Non-Sensitive Seismic Corpus

Three broadband stations of the IU network recorded a non-sensitive seismic event on 2026-05-05 (stations IU.HNR, IU.MIDW, IU.RAO, recording in the BHZ channel). Following the standard pipeline, raw waveform amplitudes are converted to the amplitude-difference sequence $\Delta A_t = A_{t+1} - A_t$ (with light smoothing), sorted into the Δ-ladder, and evaluated under STRUC-PERC-I v2.4.0. Results are given in Table 3.

Table 3: STRUC-PERC-I v2.4.0 results for three IU stations recording the 2026-05-05 seismic event (ΔA ladders).

Station	n	Verdict	GR	κ_{conn}	TD
IU.HNR (Honiara)	7,028	GIANT	0.9972	—	0.683
IU.MIDW (Midway)	1,644	FULL	1.0000	1,022	0.685
IU.RAO (Raoul Is.)	7,005	FULL	1.0000	5,016	0.608

All three stations produce admissible structures in transition space. Tail dominance values fall in the range 0.61–0.69, consistent with a heavy-tail distribution of amplitude increments: the bulk of the waveform produces moderate, uniformly distributed step sizes, while the initial P-wave arrival and secondary seismic phases contribute outlier steps that

dominate the tail. The large κ_{conn} values at IU.MIDW and IU.RAO (1,022 and 5,016 respectively) reflect the large number of elements ($n \approx 1{,}600$–$7{,}000$) rather than unusual gap structure; κ_{conn} scales with sample size for fixed gap distributions [4].

4.2 Structural Interpretation

The seismic Δ-ladder results parallel those of the supernova Δ-ladder: both produce heavy-tail admissible structures with TD ≈ 0.61–0.81 and either FULL or near-FULL percolation. The structural similarity is notable because the two physical systems differ in nearly every relevant physical quantity—energy scale, temporal duration, propagation mechanism, and generating process. Their structural proximity in the Δ-representation is consistent with the hypothesis that transition-space organization is domain-independent.

Seismic wave propagation may be understood structurally as a distributed admissible restructuring: the waveform distributes energy into a large number of moderate increments (forming the bulk of the gap distribution) with a small number of large-increment arrivals (forming the heavy tail) without breaking global structural coherence.

5 Nevada Earthquake: Representation-Distance Effects

5.1 Multi-Station Corpus

The 2026 Nevada earthquake was recorded by five stations at varying distances from the epicenter (CI.PASC, IU.ANMO, IU.COLA, IU.HRV, IU.KIP). The same ΔA ladder construction is applied uniformly. The results, summarized in Table 4, exhibit the full range of realizability classes from a single physical event.

Table 4: STRUC-PERC-I v2.4.0 results for five stations recording the 2026 Nevada earthquake (ΔA ladders), ordered by verdict severity.

Station	Location	n	Verdict	GR	κ_{conn}	TD
CI.PASC	California (local)	676	FULL	1.0000	205	0.632
IU.KIP	Kipūka, Hawai‘i	802	FULL	1.0000	84	0.193
IU.ANMO	Albuquerque, NM	253	GIANT	0.9960	—	0.000
IU.COLA	College, Alaska	193	TAIL	0.9948	—	0.070
IU.HRV	Harvard, Massachusetts	217	HARD	0.9724	—	0.095

5.2 Representation-Induced Structural Collapse

A single seismic source produces verdicts spanning the full four-class hierarchy: FULL at two proximal stations, GIANT at a mid-range station, TAIL at a distal station, and HARD at the most distant station (IU.HRV, Massachusetts, $\approx 3{,}100$ km from the Nevada epicenter). Theorem-1 is activated at IU.HRV.

This pattern is a clean demonstration of what we term *Representation-Induced Structural Collapse*:

Definition 2 (Representation-Induced Structural Collapse)**.** A system exhibits Representation-Induced Structural Collapse if its structural verdict transitions from FULL or GIANT to

HARD under a change of observational embedding that does not alter the underlying physical source, but modifies the structural observable through signal attenuation, geometric spreading, or reduced sampling resolution.

At IU.HRV, the small ladder size ($n = 217$) combined with strong geometric spreading of the waveform at teleseismic distance produces a sparse ΔA distribution in which a single large outlier gap dominates the structure, activating Theorem-1. The Nevada earthquake itself does not collapse; only the representation of the earthquake at that station does. This distinction is critical for interpreting any single-station structural assessment.

Figure 2 displays the verdict hierarchy across stations.

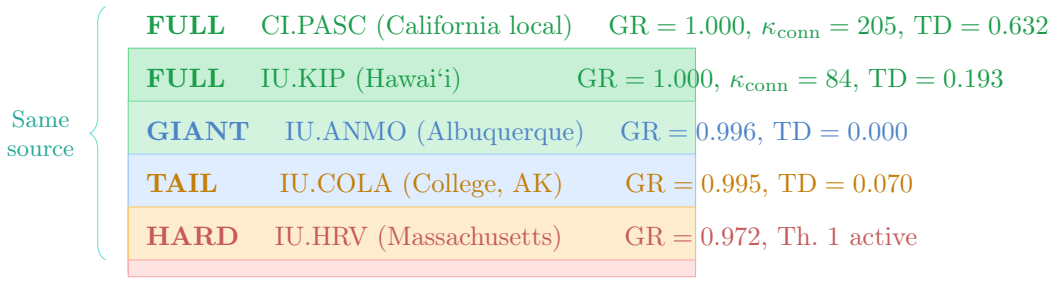

Figure 2: Nevada earthquake: STRUC-PERC-I verdicts across five stations, ranked from FULL to HARD. All stations record the same seismic source; verdict degradation is driven by propagation distance and resulting signal attenuation, not by changes in the source dynamics. This is a direct empirical demonstration of Representation-Induced Structural Collapse.

6 Nuclear Explosion Corpus: Forced Coherent Collapse

6.1 Dataset

The nuclear explosion corpus comprises seismic recordings of three events of increasing estimated yield, recorded at a network of ten broadband seismograph stations (IC.BJT, IC.HIA, IC.MDJ, IC.SSE, II.ERM, IU.INCN, IU.MAJO, IU.YSS, JP.JHJ2, JP.JNU, PS.TSK) [15]. Raw SAC waveforms are converted to amplitude-difference ladders following the standardized ΔA pipeline. Each ladder contains approximately 74,000 elements (corresponding to a 100 sps waveform over a $\sim$ 740 s analysis window), yielding robust statistical properties. In total, 29 station-event pairs are evaluated. No Theorem-1 activations are observed anywhere in the corpus.

6.2 Station-Event Verdict Heatmap

Table 5 presents the full verdict matrix, organized by station and event. Figure 3 provides the corresponding visual heatmap.

6.3 Tail Dominance Escalation with Estimated Yield

The mean tail dominance across all stations increases monotonically with estimated event yield: $\overline{\text{TD}}_{E1} = 0.753$, $\overline{\text{TD}}_{E2} = 0.827$, $\overline{\text{TD}}_{E3} = 0.886$. This monotonic escalation is consis-

Table 5: STRUC-PERC-I v2.4.0 verdicts and tail dominance for the nuclear explosion seismic corpus (29 station-event pairs). Event 1: estimated yield $\sim$ 1 kt; Event 2: $\sim$ 2–6 kt; Event 3: $\sim$ 6–40 kt. G: GIANT, T: TAIL. All giant ratios > 0.97. No Theorem-1 activations. Stars ($\star$) mark IC.MDJ (station closest to source).

	Event 1			Event 2			Event 3		
Station	V	GR	TD	V	GR	TD	V	GR	TD
IC.BJT	G	0.997	0.556	G	0.995	0.825	T	0.994	0.878
IC.HIA	G	0.997	0.723	G	0.996	0.842	T	0.994	0.936
IC.MDJ$\star$	T	0.980	0.990	T	0.971	0.996	T	0.975	0.997
IC.SSE	G	0.997	0.589	G	0.997	0.599	G	0.997	0.710
II.ERM	G	0.997	0.656	G	0.996	0.767	T	0.994	0.811
IU.INCN	T	0.995	0.803	T	0.992	0.927	—	—	—
IU.MAJO	G	0.996	0.818	T	0.990	0.915	T	0.984	0.978
IU.YSS	G	0.996	0.802	G	0.996	0.744	G	0.996	0.855
JP.JHJ2	—	—	—	G	0.997	0.704	T	0.992	0.855
JP.JNU	—	—	—	T	0.987	0.958	T	0.986	0.955
PS.TSK	T	0.994	0.844	T	0.994	0.819	—	—	—

tent across the majority of individual stations: of the nine stations with data for all three events, seven exhibit $\mathrm{TD}_{E1} < \mathrm{TD}_{E2} < \mathrm{TD}_{E3}$.

Figure 4 illustrates this yield-dependent escalation alongside the corresponding station-level tail dominance at IC.MDJ.

6.4 IC.MDJ Structural Saturation

Station IC.MDJ (Mudanjiang, China; estimated epicentral distance ≈ 360 km, the closest network station to the source) exhibits TAIL-class verdicts for all three events, with tail dominance reaching TD = 0.990, 0.996, and 0.997 for Events 1, 2, and 3 respectively. Despite this near-total saturation of gap mass in the outlier tail, the giant ratio remains $\mathrm{GR} \in [0.971, 0.980]$ across all three events, and Theorem-1 is never activated.

This coexistence of extreme tail domination and preserved global connectivity is the defining feature of the Forced Coherent Collapse regime.

6.5 Forced Coherent Collapse

The nuclear explosion corpus motivates the following structural definition, which formalizes the coexistence of extreme tail loading and preserved global connectivity observed at IC.MDJ and throughout the 2013 event.

Definition 3 (Forced Coherent Collapse)**.** A ladder L (or a family of ladders derived from the same physical process) belongs to the *Forced Coherent Collapse* (FCC) regime under STRUC-PERC-I evaluation if it simultaneously satisfies:

(i) **Tail-dominated gap structure.** The gap distribution is dominated by a small number of extreme outlier gaps:

$$\mathrm{TD}(L) > 0.80,$$

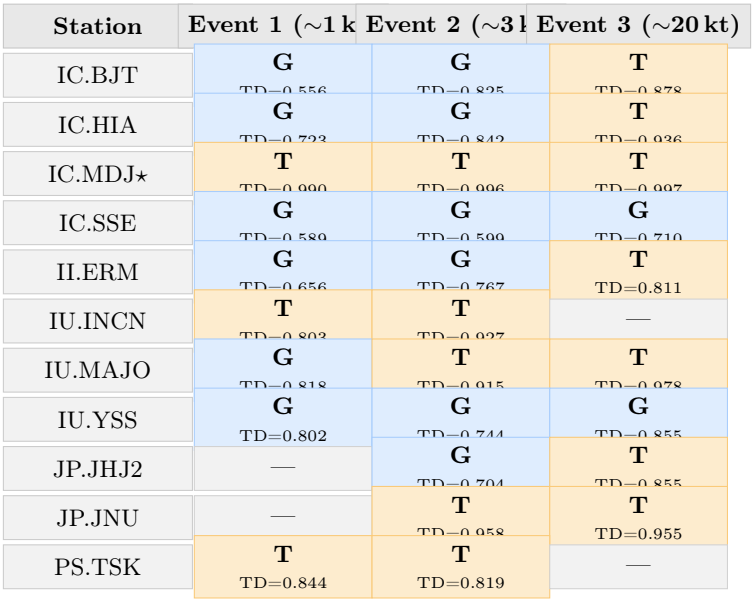

Figure 3: NK explosion corpus: STRUC-PERC-I v2.4.0 verdict heatmap. G: GIANT, T: TAIL. Color encodes verdict class; internal labels show tail dominance. IC.MDJ (⋆) is the station closest to the source and shows TAIL with TD > 0.99 across all three events. No Theorem-1 (HARD) activations are observed anywhere in the corpus. Missing entries indicate no available data for that station-event pair.

where TD is the fraction of total gap mass carried by gaps exceeding $10 \times \text{median}(\delta)$. In extreme cases TD approaches saturation (≈ 0.99–1.0).

(ii) **Preserved giant-component connectivity.** A dominant backbone giant component persists across the full κ-scale sweep:

$$\text{GR}(L, \kappa) \;\geq\; \text{GR}_{\text{thresh}} \quad \forall\, \kappa \in \mathcal{K},$$

with $\text{GR}_{\text{thresh}} = 0.97$ (typically the giant component retains the large majority of vertices throughout).

(iii) **Absence of hard fragmentation.** No Theorem-1 activation occurs: there are no persistent isolated vertices or multi-component fragmentation surviving the full κ-sweep; the system never enters the HARD class.

A system in FCC is *collapsed* in gap space—a tiny fraction of transitions carry the majority of structural weight—while remaining *coherent* in connectivity space: the vulnerability graph maintains a spanning giant component even under extreme tail loading.

The qualifier *forced* describes the physical situation: extreme tail dominance is imposed by the nature of the process (a powerful, localized energy release generating a few very large amplitude steps amid many smaller ones), not by a structural failure of the system. The qualifier *coherent* reflects that the bulk connectivity backbone survives this forcing: enough moderate-scale connections remain to maintain a giant component.

Why FCC is not merely extreme Tail. Ordinary TAIL-class ladders exhibit high tail dominance and high but sub-unity giant ratios, and their structural trajectory under

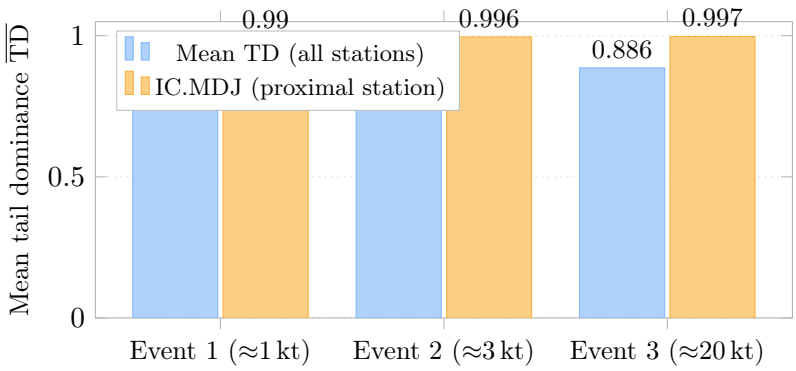

Figure 4: Mean tail dominance per event across all stations (blue) and for the proximal station IC.MDJ (amber). Both series increase monotonically with estimated event yield. IC.MDJ saturates near TD = 0.997 for Event 3, yet the giant component is maintained (GR > 0.97) throughout the corpus.

increasing forcing is, in general, ambiguous: more extreme tail loading can either push GR lower (toward HARD) or allow it to remain stable. FCC identifies the specific case where GR remains robustly stable—at or above 0.97—as TD approaches saturation. It is not simply "very strong Tail"; it is Tail with a demonstrated connectivity floor. The structural distinction is that ordinary Tail approaches fragmentation as TD $\to$ 1, while FCC approaches tail saturation while the giant component is preserved. This places FCC at the upper-right frontier of the TAIL regime in the (TD, GR) atlas: maximum tail loading without crossing the HARD boundary. Table 6 summarizes the five-regime taxonomy.

Table 6: Structural regime taxonomy under STRUC-PERC-I. FCC occupies the upper-right frontier of the Tail regime—extreme tail loading without crossing into Hard fragmentation.

Regime	TD	GR	Th. 1	Structural interpretation
FULL	low–mod	$= 1.000$	No	Globally connected; balanced gaps
GIANT	low–mod	≈ 1	No	Strong backbone + bounded isolates
TAIL	high	high < 1	No	Heavy tail; connected but gap-domina
FCC	**very high (≥ 0.80, often $\to 1$)**	≥ 0.97	**No**	**Extreme tail forced by physics; b**
HARD	variable	$< \text{GR}_{\text{thresh}}$	Yes	True fragmentation / collapse

The canonical realization in this corpus is the IC.MDJ station across all three events (Table 5): TD ≥ 0.990, GR $\in [0.971, 0.980]$, zero Theorem-1 activations. Physical interpretation: the extreme seismic arrivals from a nearby nuclear release generate a few very large amplitude steps that dominate the gap statistics, while the remaining waveform provides sufficient moderate-scale connections to maintain global structural coherence.

Observation 2 (FCC in the nuclear explosion corpus)**.** Across 29 station-event pairs, zero HARD-fragmentation verdicts are observed. The proximal station IC.MDJ exhibits Forced Coherent Collapse with TD ≥ 0.990 and GR ≥ 0.971 for all three events. Mean tail dominance escalates monotonically with estimated yield: $0.753 \to 0.827 \to 0.886$.

6.6 Mathematical Properties of the FCC Regime

We derive six properties from the operational definition (Definition 3). Let the ordered gaps of the ladder be $g_1 \le g_2 \le \cdots \le g_{n-1}$ with total gap mass $S = \sum_i g_i$, and let $T = \{i : g_i > 10 \cdot \text{median}(g)\}$ denote the outlier index set.

Proposition 2 (Tail Saturation Bound)**.** *In FCC, there exists a small set of extreme gaps such that*

$$\frac{\sum_{i \in T} g_i}{S} \;\ge\; \tau, \quad |T| \ll n-1,$$

*where $\tau = 0.80$ is the FCC threshold. For extreme FCC (*TD $\to 1$*), the largest m gaps satisfy $\sum_{i=n-m}^{n-1} g_i \approx S$, implying $\text{mean}(g_{small}) \ll \text{mean}(g_{large})$. This is consistent with a bimodal or power-law-like gap distribution with a heavy upper tail, structurally characteristic of impulsive processes.*

Proposition 3 (Connectivity Margin Preservation)**.** *Even with extreme tail dominance, the vulnerability graph $G_\kappa(L)$ maintains*

$$\text{GR}(\kappa) \;\ge\; \gamma \quad \forall\, \kappa \in [\kappa_{\min}, \kappa_{\text{conn}}^{\text{FCC}}]$$

for $\gamma = 0.97$. The mechanism is that moderate gaps (the non-tail bulk) form a sufficiently dense background chain in the ordered ladder. Extreme gaps act as potential separators at low κ, becoming connectable as κ grows: in a 1D-embedded ladder, removing or rescaling a few large gaps does not shatter the chain if the remaining points satisfy a bounded-gap condition. As a heuristic estimate for fractional tail size $f = |T|/(n-1)$,

$$\text{GR} \;\gtrsim\; 1 - c \cdot f \cdot \log n$$

for a small constant c (not rigorously derived; serves as a structural illustration of why GR *remains ≥ 0.97 even at* TD > 0.95 *when f is small). The formal derivation of this bound requires a graph-theoretic specification of the vulnerability graph and asymptotic assumptions on gap distributions not imposed here.*

Proposition 4 (Boundary with Hard Fragmentation)**.** *FCC lies immediately adjacent to the* HARD *regime in the* (TD, GR) *phase plane. The transition occurs when tail gaps become so dominant that they isolate vertices or create persistent disconnected clusters (Theorem-1 trigger). The structural margin of an FCC system,*

$$m_{\text{FCC}}(L) \;=\; \textit{minimal gap-rescaling perturbation to drop } \text{GR} < \gamma \textit{ or trigger Th. 1},$$

is small but positive. Conversely, the Δ-lifting often reduces effective TD *and restores higher* GR/FULL *regimes, increasing m_{FCC} substantially.*

Proposition 5 (Δ-Representation and Giant-Ratio Stabilization)**.** *Applying the first-difference operator $L \mapsto L^\Delta$ typically improves or preserves giant-component connectivity:*

$$\text{GR}(L^\Delta) \;\ge\; \text{GR}(L),$$

because differencing removes global scale offsets and baseline drifts that create dominant gaps in the raw-state embedding. However, TD(L^Δ) *may be* greater or less than TD(L),

depending on whether the transform concentrates transition structure into fewer dominant gaps (increasing TD*) or disperses it (decreasing* TD*).* Example (SN Ia): *The raw magnitude ladder has* TD $= 0.309$ *(one dominant bright-end gap); the* Δ*-magnitude ladder has* TD $= 0.811$ *(many comparable-scale flux increments with a few outliers). Here* GR *improves from* 0.952 *to* 1.000 *while* TD *increases substantially—the* Δ*-lifting transfers the structural burden from a single non-representative gap to an admissible heavy-tail distribution.* Example (NK corpus): *In* ΔA *seismic ladders, both* GR *and* TD *are high, consistent with FCC. The* Δ*-representation stabilizes* GR*;* TD *reflects the physical impulsive structure, not a representation artifact. The net consequence is that the* Δ*-layer is a structural* connectivity *stabilizer, not a tail-reduction operator.*

Proposition 6 (Yield–TD Saturating Scaling)**.** *Model the observed amplitude* A *of the dominant seismic phases at a fixed station as* $A \propto Y^{\alpha}$ *for estimated yield* Y *(*$\alpha \approx \frac{1}{3}$–$\frac{2}{3}$*, consistent with body-wave magnitude scaling* $m_b \approx \frac{2}{3}\log_{10} Y + c$*). With* k *dominant tail gaps scaling as* $g_t^{(i)} \approx c_0 Y^{\alpha}$ *and a background sum* $S_b = n_b \mu_b$ *that is yield-independent (or weakly so), the total gap sum is* $S(Y) = S_b + k c_0 Y^{\alpha}$ *and tail dominance takes the saturating (Michaelis-Menten) form:*

$$\mathrm{TD}(Y) \;=\; \frac{\beta Y^{\alpha}}{1+\beta Y^{\alpha}}, \qquad \beta = \frac{k c_0}{n_b \mu_b}. \tag{8}$$

Conditional monotonicity. *Under the stated model assumptions (tail gaps scale positively with* Y*; background statistics yield-independent;* k *fixed or slowly growing), differentiating* (8) *gives*

$$\frac{d\,\mathrm{TD}}{dY} \;=\; \frac{\beta\alpha Y^{\alpha-1}}{(1+\beta Y^{\alpha})^2} \;>\; 0$$

for all $\alpha > 0$*,* $\beta > 0$*,* $Y > 0$*. Hence* TD *is strictly increasing in* Y *within the model.* Saturation behavior. *At low* Y*:* TD $\approx \beta Y^{\alpha}$ *(power-law growth). At high* Y*:* TD $\to 1$ *(saturation). This matches IC.MDJ:* TD *rises from* 0.990 *(Event 1,* $\sim$*1 kt) to* 0.997 *(Event 3,* $\sim$*20 kt). For practical fitting at intermediate yields, before full saturation, a log-linearization applies:* $\mathrm{TD}(Y) \approx a + b\log_{10} Y$*.* Giant-ratio stability (Corollary). *Because the background ladder remains dense (coda structure maintained), the giant component is preserved (*GR ≥ 0.97*) even as* TD $\to 1$*: tail gaps become bridgeable thresholds at sufficient* κ *(Structural Argument 1), not as isolators.* Phase-plane trajectory. *In the* (TD, GR) *atlas, increasing yield traces a rightward path along the upper Tail frontier:* TD $\uparrow$ *(forcing) while* GR $\approx$ const *(coherence preserved)—the dynamical signature of Forced Coherent Collapse. Mean corpus trajectory:* $\overline{\mathrm{TD}}_{E1} = 0.753 \to \overline{\mathrm{TD}}_{E2} = 0.827 \to \overline{\mathrm{TD}}_{E3} = 0.886$*, with* GR *varying only within* $[0.971, 0.997]$*.*

Proposition 7 (Effective κ-Threshold Shift)**.** *The connectivity threshold required for giant-component formation is elevated in FCC relative to balanced-gap ladders of the same size:*

$$\kappa_{\mathrm{conn}}^{\mathrm{FCC}} \;>\; \kappa_{\mathrm{conn}}^{\mathrm{balanced}},$$

reflecting the need to bridge extreme outlier gaps with the background connectivity. However, $\kappa_{\mathrm{conn}}^{\mathrm{FCC}}$ *remains finite within the tested* κ*-range—in contrast to* Hard *fragmentation, where no* κ *within the evaluated structural scale range restores spanning connectivity (Theorem-1 activation persists across the full tested grid). This within-range distinction is the oper-*

ational separation between FCC and HARD *under STRUC-PERC-I: global coherence is recoverable in FCC at a κ value accessible within the instrument's scale sweep.*

Proposition 8 (Distance–TD Attenuation Model)**.** *For body-wave seismic arrivals (P_n, L_g) at regional distances, the peak amplitude attenuates as*

$$A(d) \;\propto\; Y^{\alpha} \cdot G(d) \cdot e^{-\gamma d},$$

where $G(d) \sim d^{-\beta_G}$ ($\beta_G \approx 0.5$–1) is geometric spreading and $\gamma = \pi f/(Qv)$ is the anelastic coefficient (empirical values $Q \approx 200$–500 for P_n/L_g). Let $\beta(d) = kc_0 Y^{\alpha} G(d) e^{-\gamma d}/(n_b \mu_b)$. Tail dominance at distance d takes the form

$$\mathrm{TD}(d) \;=\; \frac{\beta(d)}{1+\beta(d)},$$

where $\beta(d)$ is a decreasing function of d (since $G(d)e^{-\gamma d}$ is strictly decreasing for $\gamma > 0$, $\beta_G > 0$). Conditional monotonicity. *Differentiating under the stated attenuation model:*

$$\frac{d\,\mathrm{TD}}{dd} \;=\; \frac{\beta'(d)}{(1+\beta(d))^2} \;<\; 0,$$

since $\beta'(d) < 0$. Hence, under the model, TD *is strictly decreasing in d.* Near-source saturation. *At short epicentral distances ($d \to d_{\min}$), $\beta(d) \gg 1$ and* TD $\to 1$ *(extreme FCC, as observed at IC.MDJ ≈ 360 km). At larger distances,* TD *decays toward ordinary* TAIL *or moderate values, while* GR *remains above* 0.97 *(no* HARD *outcomes across the tested corpus).* Prediction. *After yield normalization,* TD *should correlate negatively with epicentral distance across any network of stations recording the same explosion event. The nuclear explosion corpus is consistent with this prediction (IC.MDJ highest* TD*; distant stations lower* TD*; all* GR ≥ 0.97*).*

Propositions 6 and 8 treat source-strength scaling and distance attenuation separately, as domain-specific instances within the nuclear explosion corpus. The following proposition unifies them into a single two-parameter scaling law that extends across all three extreme-transition domains of this manuscript. It constitutes the first cross-domain transport law of FCC/Tail realizability in the UNNS framework: where earlier results described static structural states, this proposition describes how realizability class evolves under propagation.

Proposition 9 (Unified Tail Dominance Scaling Law)**.** *In impulsive coherent systems analyzed via gap ladders (amplitude-difference, energy-difference, or curvature representations), tail dominance* TD *obeys the saturating scaling form under joint variation of source strength S and effective propagation distance d:*

$$\mathrm{TD}(S,d) \;=\; \frac{\beta_0 \cdot \phi(S) \cdot \psi(d)}{1+\beta_0 \cdot \phi(S) \cdot \psi(d)}, \tag{9}$$

where:

- *S: source strength parameter (yield Y for explosions; seismic moment $M_0 \propto 10^{1.5M}$ for earthquakes; peak luminosity or ^{56}Ni mass for supernovae);*

- *d: effective propagation distance (epicentral distance for seismic; luminosity distance or redshift z for supernovae);*
- *$\phi(S) \propto S^{\alpha}$ with $\alpha > 0$ (source scaling; $\alpha \approx \frac{1}{3}$–$\frac{2}{3}$ for seismic amplitude);*
- *$\psi(d)$: attenuation/dimming function, strictly decreasing ($\psi'(d) < 0$); for seismic: $\psi(d) = d^{-\beta_G} e^{-\gamma d}$; for supernovae: $\psi(z) \propto (1+z)^{-\delta}$ (flux dimming plus time-dilation stretch);*
- *$\beta_0 > 0$: system-specific constant encoding background gap statistics, number of dominant tail events k, and instrumental factors.*

Conditional monotonicity. *Under the stated model:*

$$\frac{\partial\,\mathrm{TD}}{\partial S} > 0 \quad \textit{(TD increases with source strength)}, \qquad \frac{\partial\,\mathrm{TD}}{\partial d} < 0 \quad \textit{(TD decreases with distance/redshift)}.$$

Both follow by direct differentiation of (9): $\partial T/\partial S > 0$ and $\partial T/\partial d < 0$ (since ϕ is increasing and ψ is decreasing), with the denominator always positive.

Limit behavior. *At high source strength and short propagation distance ($\beta_0\phi\psi \gg 1$):* $\mathrm{TD} \to 1$ *(extreme FCC; IC.MDJ,* $\mathrm{TD} = 0.997$*). At large distance or weak forcing ($\beta_0\phi\psi \ll 1$):* $\mathrm{TD} \approx \beta_0\phi(S)\psi(d)$ *(power-law regime; ordinary* Tail*).*

Giant-ratio preservation. *Under the background connectivity assumption (coda phases, scattered arrivals, or moderate flux variations provide dense moderate-scale gaps satisfying the bounded-gap condition of Structural Argument 1):*

$$\mathrm{GR}(S, d) \;\geq\; \gamma \;=\; 0.97$$

across the physically relevant range of (S, d). Tail gaps are potential separators at low κ, but become bridgeable thresholds once the background chain provides dense local coverage and κ reaches the tail-gap scale, strongly suppressing transition to persistent Hard *fragmentation under the bounded-connectivity assumption.*

Connection to margin transport. *The observable quantity* TD *is the phase-plane projection of a deeper structural coordinate: the connectivity margin $m(L_t)$ (Definition 1) evaluated along the propagation trajectory (S, d). As (S, d) varies, $m(L_t)$ changes continuously, tracing a path through the admissibility manifold $\mathcal{M}_{\mathrm{adm}}$.* TD *measures the gap-mass concentration along this path; $m(L_t)$ encodes the boundary distance. The transport law (9) therefore describes realizability transport in $\mathcal{M}_{\mathrm{adm}}$ under propagation—a dynamical extension of the static classification framework.*

Domain specializations.

- ***Nuclear explosions.*** *$\phi(Y) = Y^{\alpha}$, $\psi(d) = d^{-\beta_G} e^{-\gamma d}$. Canonical FCC at proximal stations; Props. 6 and 8 are special cases.*
- ***Natural earthquakes.*** *$\phi(M_0) \propto 10^{M}$; same $\psi(d)$ with stronger scattering term. Higher variability from rupture directivity and site effects; proximal strong-motion records realize FCC, teleseismic records shift toward* Hard *(RISC).*
- ***Supernova light curves.*** *$\phi(S) \propto L_{\mathrm{peak}}^{\eta}$; $\psi(z) \propto (1+z)^{-\delta}$ (flux dimming + time dilation). Δ-energy and curvature ladders recover FCC/*Tail*; raw magnitude ladders show RISC. Low-z events realize stronger FCC-like structure.*

Falsifiable predictions. *This scaling law predicts: (i)* TD *should correlate negatively with redshift in larger ZTF supernova samples; (ii)* TD *should decay monotonically with hypocentral distance in regional earthquake networks after yield/magnitude normalization; (iii) proximal nuclear explosion recordings saturate* TD $\to 1$ *while* GR *remains bounded below* 0.97. *All three are directly testable with existing public data archives.*

6.7 Structural Connectivity Argument

The following is a structural heuristic argument—not a formal mathematical proof—for why FCC systems maintain giant-component connectivity under extreme tail loading. It serves as geometric intuition for Definition 3, Proposition 1, and Propositions 3–9, and underpins the GR-preservation clause of the Unified Scaling Law (Proposition 9). A rigorous proof would require a formal specification of the vulnerability graph model, asymptotic assumptions on gap distributions, and measure-theoretic control not provided here.

Structural Argument 1 (1D Chain: Background Connectivity Under Tail Forcing)**.** Let $L = \{x_1 < x_2 < \cdots < x_n\}$ on $\mathbb{R}$ with gaps $g_i = x_{i+1} - x_i$. Let T denote the index set of outlier (tail) gaps with $|T| = k \ll n$, and $B = \{1, \ldots, n-1\} \setminus T$ the background gaps. Assume the bounded-gap condition: $\max_{i \in B} g_i \leq \kappa_0$ for some moderate κ_0.

1. **Background chain.** The subsequence of points connected by background gaps forms an (approximately) connected path with steps $\leq \kappa_0$. Its induced subgraph in G_κ for $\kappa \geq \kappa_0$ has at least $n - k$ vertices in a single connected component. The giant component is at least as large: GR $\geq (n-k)/n = 1 - f$, where $f = k/n$ is the tail fraction.

2. **Tail gaps as bridgeable thresholds.** Each tail gap $g_i \in T$ spans a large distance but does not isolate vertices: in the sorted 1D ordering, both endpoints of a large gap are already embedded in the background chain on either side. At low κ, tail gaps can act as separators; once κ reaches the tail-gap scale, they become connected thresholds. In the 1D-sorted ordering, both endpoints of a large gap lie in the background chain, so the gap is bridgeable rather than permanently disconnecting. Under moderate κ (between κ_0 and the tail-gap scale), the background chain provides local density while tail gaps provide global bridging.

3. **Component counting.** At κ below the tail-gap scale, the number of disconnected components is bounded by the number of tail gaps plus one: #components $\leq k + 1$. The largest component therefore contains at least $n/(k+1)$ vertices, which is $\gg n/2$ for small k. Once κ exceeds κ_0, background connectivity recovers; once κ exceeds the characteristic tail-gap scale, the tail gaps are bridged and GR $\to 1$.

4. **Structural margin.** To transition into HARD fragmentation, a tail gap must grow (or κ must shrink) until it permanently isolates at least one vertex across the full κ-sweep. The margin to this boundary is positive but small, scaling heuristically with $\max(g_T)/n$ — hence FCC systems are near-critical: "forced" by the outlier structure but "coherent" because the background chain keeps the margin positive.

5. **Effect of Δ-lifting.** Applying Δ replaces absolute-scale gaps g_i with local differences $\Delta g_i = g_{i+1} - g_i$, removing global baseline offsets. This typically improves GR by eliminating dominant embedding artifacts, increasing the structural margin and moving the system further from the HARD boundary. TD may increase or decrease depending on whether the transform concentrates or disperses transition structure—consistent with Proposition 5.

The intuitive summary is: the background bulk provides local connectivity density; the tail provides extreme but non-destructive forcing; together they produce the FCC signature of high TD with preserved GR.

6.8 Physical Mechanism, Proximity Effect, and Seismological Extension

The structural properties of the FCC regime are realized physically through a specific waveform geometry characteristic of impulsive seismic sources. This section explains the physical mechanism generating FCC in the nuclear explosion corpus, the spatial structure introduced by the proximity effect, and the extension of the FCC interpretation to natural impulsive seismic events.

6.8.1 Waveform Structure and the FCC Mechanism

A nuclear explosion generates a sharply impulsive pressure wave that propagates through the crust as seismic energy. In the resulting ground-motion record, the waveform decomposes into two structurally distinct components:

1. **Impulsive phases ($\mathbf{P}_n$, $\mathbf{L}_g$, main shock).** The initial compressional wave and the largest seismic phases produce a small number of very large amplitude steps in the ΔA sequence. These become the outlier gaps in the structural ladder, driving TD toward saturation. Physically, this is the "forced" component of FCC: the extreme energy release is concentrated into a few amplitude transitions.

2. **Coda and secondary phases.** The extended coda train—scattered energy propagating via multiple reflection and refraction paths—generates a large number of moderate amplitude increments. These fill the background of the ΔA distribution and form the dense chain that preserves giant-component connectivity. Physically, this is the "coherent" component of FCC: the propagating wavefield maintains distributed structural coverage that prevents the background chain from breaking.

The structural argument of Section 6.7 directly parallels this physical decomposition: the background chain corresponds to the coda, and the tail gaps correspond to the impulsive phases becoming bridgeable at sufficient κ.

6.8.2 The Proximity Effect

Station IC.MDJ, at an estimated epicentral distance of ≈ 360 km, is the closest station in the network to the source. At this distance, seismic waves have undergone less geometric spreading and anelastic attenuation than at more distant stations. Two structural consequences follow:

1. **Stronger tail dominance.** Less attenuation means the impulsive phases arrive with higher amplitude relative to the coda, amplifying the outlier gaps and pushing TD toward saturation (0.990–0.997 across all three events).

2. **Preserved coherence.** The coda energy at short range is also stronger, maintaining the background chain that supports giant-component connectivity. GR at IC.MDJ (0.971–0.980) is actually slightly lower than at some distant stations, reflecting the stronger tail forcing, but remains firmly within the FCC zone (GR ≥ 0.97).

This gives FCC spatial structure: proximity to the source organizes stations along a trajectory of increasing TD with approximately stable GR, tracing the upper frontier of the Tail regime from the moderate-FCC zone (distant stations) toward near-saturation (IC.MDJ). The proximity effect transforms FCC from a static label into a spatially organized transition geometry.

Observation 3 (Proximity-TD Relationship)**.** Within the nuclear explosion corpus, proximal stations (shorter epicentral distance, less propagation attenuation) exhibit higher tail dominance than distal stations for the same event, while maintaining GR ≥ 0.97 throughout. IC.MDJ (≈ 360 km) consistently achieves TD ≥ 0.990 across all three events, while more distant stations such as IC.SSE show TD ≤ 0.71 for the same events.

6.8.3 The Yield Trajectory in the $(\mathrm{TD}, \mathrm{GR})$ Atlas

The yield-intensity scaling (Proposition 6) acquires a geometric interpretation in the $(\mathrm{TD}, \mathrm{GR})$ atlas. As estimated event yield increases from Event 1 ($\sim$1 kt) through Event 3 ($\sim$20 kt), the mean corpus position traces a rightward trajectory in the atlas: increasing TD ($0.753 \to 0.827 \to 0.886$) with nearly constant GR (≈ 0.97–1.00). At IC.MDJ specifically, this trajectory reaches TD $= 0.997$ while GR holds at 0.975.

This turns FCC from a static classification into a *dynamical trajectory regime*: a sequence of physical states connected by increasing source strength, all lying along the upper Tail frontier, none crossing into HARD fragmentation. The trajectory terminates at the HARD boundary if and when tail gaps become large enough to permanently isolate vertices; the empirical observation that this does not occur even at the highest tested yield ($\sim$20 kt) is itself a structural result.

6.8.4 Nuclear Explosions vs. Natural Earthquakes: A Structural Contrast

The comparison between the nuclear explosion corpus (Section 6) and the Nevada earthquake corpus (Section 5) reveals a structurally important distinction between impulsive and distributed seismic sources.

Nuclear explosions are structurally "cleaner" impulsive sources: a single, highly localized detonation generates a brief, high-amplitude wavelet followed by an extended coda. This waveform geometry maps directly onto the FCC mechanism: few extreme tail gaps (from the impulsive onset) and many moderate background gaps (from the coda). The result is systematic FCC across all station-event pairs, with zero HARD outcomes regardless of station distance or event yield.

Natural earthquakes involve distributed rupture along an extended fault plane. The rupture heterogeneity introduces multiple strong seismic phases at irregular timing intervals, and at teleseismic distances the signal undergoes complex scattering that can dramatically alter the gap distribution. The Nevada earthquake (Section 5) demonstrates this: the same event produces FULL percolation at proximal stations and HARD fragmentation (Representation-Induced Structural Collapse) at teleseismic distances. Where nuclear explosions produce clean FCC, natural earthquakes may produce either FCC (at proximal stations with good signal-to-noise), ordinary TAIL or GIANT (at intermediate distances), or Representation-Induced HARD (at teleseismic distances).

Observation 4 (Structural Contrast: Explosion vs. Earthquake)**.** In the tested corpus, nuclear explosion seismic signals realize FCC systematically across all station-event pairs, reflecting the clean impulsive source structure. Natural earthquake signals (Nevada) produce a full verdict spectrum (FULL to HARD) depending on propagation distance, reflecting the representation-distance sensitivity introduced by distributed rupture and teleseismic attenuation. The structural distinction between these source types is operationally detectable in the ΔA ladder verdict without reference to source mechanism or magnitude.

6.8.5 Extension to General Impulsive Seismicity

The FCC mechanism generalizes beyond the nuclear explosion corpus to any impulsive seismic source at suitable station distance:

Observation 5 (FCC in Impulsive Seismicity)**.** In impulsive seismic events (explosions or rupture-like earthquakes at proximal stations), waveform ΔA ladders are expected to realize the FCC regime: TD escalates with source strength and proximity while GR ≥ 0.97 and Theorem-1 is suppressed. This is the structural signature of coherent energy propagation under extreme localized release: the physics generates outlier gaps (impulsive phases) without destroying the background connectivity provided by the coda and secondary arrivals. The prediction is directly testable: Δ-envelope or curvature ladders from regional seismic networks should map closer stations and stronger events into the FCC zone of the (TD, GR) atlas, while distant stations should map toward ordinary TAIL or Representation-Induced HARD.

This prediction extends the empirical scope of the FCC definition beyond the current corpus without asserting universality. It is falsifiable by any broadband seismic dataset in which proximal recordings of impulsive events fail to show TD > 0.80 and GR ≥ 0.97 simultaneously.

7 Cross-Domain FCC Comparison: Nuclear Explosions, Supernovae, and Earthquakes

The FCC regime, established empirically from the nuclear explosion corpus, has structural analogs in the two other extreme-transition domains of this manuscript: the type Ia supernova ZTF20acobvxk and the Nevada earthquake network. The comparison reveals both shared structural mechanisms and important source-dependent distinctions, together establishing the scope and limits of FCC as a cross-domain structural regime.

7.1 Forcing Parameter and Tail Dominance Behavior

In each domain, a physical forcing parameter drives tail dominance in transition-space ladders:

- **Nuclear explosions.** Event yield Y is the forcing parameter. Tail dominance increases monotonically with Y following the saturating form of Proposition 6, and decreases monotonically with epicentral distance d following Proposition 8. The result is a two-parameter phase surface in (Y, d) space, with FCC (high TD, preserved GR) realized at high yield and short distance. This is the cleanest realization: a controlled point-source impulse with predictable attenuation behavior.

- **Supernova light curves.** Luminosity (determined by ^{56}Ni mass and ejecta velocity) plays an analogous role to yield. Higher luminosity corresponds to larger outlier gaps in Δ-energy ladders (larger flux steps at peak and decline). Cosmological redshift z acts as a compound "distance" parameter: it attenuates flux (analogous to geometric spreading) and stretches the light curve by $(1+z)$ (analogous to temporal broadening). At low z, well-sampled nearby supernovae with strong peaks realize FCC-like signatures (TD > 0.75, GR near unity) in Δ-energy and curvature ladders. The critical difference from nuclear explosions is that raw-state representations (sorted magnitudes) frequently produce Representation-Induced Structural Collapse (HARD), while the Δ-lifting recovers FULL percolation. Nuclear explosions, by contrast, remain in TAIL/GIANT (never HARD) even in the ΔA representation.

- **Natural earthquakes.** Earthquake magnitude plays the role of a forcing parameter analogous to yield, but with substantially greater variability due to rupture complexity, directivity, and site effects. At proximal stations, impulsive rupture onset (P-wave) creates large outlier gaps; the coda provides background connectivity. FCC-like signatures are expected at short distances for strong events. The key structural distinction is that earthquakes involve distributed shear rupture (double-couple mechanism) rather than the isotropic point-source detonation of a nuclear explosion. This introduces directivity-dependent amplitude variation and richer secondary phases—both of which increase the variability of the gap distribution and raise the risk of Representation-Induced Structural Collapse at teleseismic distances, as directly observed in the Nevada corpus (IU.HRV: HARD, $n = 217$).

7.2 Comparative Structural Table

Table 7 summarizes the three-domain structural comparison.

7.3 Structural Implications of the Comparison

Three structural conclusions follow from the comparison:

Nuclear explosions as a controlled FCC laboratory. The combination of controlled yield, predictable attenuation, and clean point-source geometry makes nuclear explosion seismic signals the most direct realization of FCC available in this corpus. The yield and distance parameters independently tune the forcing along analytically tractable trajectories

Table 7: Cross-domain structural comparison: FCC behavior under extreme transitions in three physically distinct systems. RISC: Representation-Induced Structural Collapse.

Structural aspect	Nuclear explosions	Supernova (SN Ia)	Natural earthquakes
Forcing parameter	Yield Y (controlled)	Luminosity / Ni mass (intrinsic)	Magnitude / rupture area
"Distance" effect	Strong TD ↓ with d; geometric + anelastic attenuation	TD ↓ with redshift z; flux dimming + time dilation	TD ↓ with distance; stronger scattering than nuclear
Proximal signature	Extreme FCC (TD ≈ 0.99+, GR ≥ 0.97)	Stronger Tail/FCC in Δ-energy (low-z events)	FCC-like at near-field stations
Distant signature	Milder Tail; still coherent (GR ≥ 0.97); no HARD	Compressed TD; raw-state HARD (RISC); recovered by Δ-lifting	Higher risk of RISC; HARD at teleseismic distances
Raw-state verdict	TAIL/GIANT (no HARD in ΔA)	HARD (Theorem-1 in raw magnitude)	Mixed: FULL to HARD by station
Δ-lifting effect	Stabilizes GR; TD may increase or decrease	Recovers FULL percolation (κ_{conn} = 141–185)	Recovers FULL/GIANT at proximal stations
Coherence robustness	Very robust (zero HARD across 29 pairs)	Representation-dependent; robust in Δ-layer	More variable; path-dependent
Canonical UNNS regime	FCC (canonical realization)	FCC/TAIL (representation-dependent)	TAIL → FCC (proximal) or HARD (distant)

(Propositions 6 and 8), and the absence of HARD outcomes across all 29 station-event pairs confirms that the FCC connectivity floor is robustly maintained.

Supernovae require Δ-lifting to reveal FCC-like structure. Raw-state supernova representations produce Representation-Induced Structural Collapse (HARD, Theorem-1 active) because the absolute-magnitude embedding places a large bright-end gap in the ladder that persistently prevents percolation. The Δ-lifting removes this embedding artifact and recovers FULL percolation with κ_{conn} = 140–185, consistent with FCC-like tail structure (TD = 0.755–0.811). The difference from nuclear explosions is that Δ-lifting is a necessary step for supernovae, not just a stabilizing one. This reinforces the central thesis: the Δ-representation is the correct structural observable for absolute-scale time series.

Earthquakes exhibit representation-distance fragility absent in nuclear sources. The Nevada earthquake corpus shows that distributed rupture mechanisms, combined with teleseismic propagation, produce a structural verdict spectrum that nuclear explosions do not. This fragility has a physical interpretation: earthquake ruptures generate a wider variety of seismic phase amplitudes (stronger S-wave content, directivity lobes, variable

site amplification) than the isotropic nuclear source, making the gap distribution less predictably bimodal and more susceptible to RISC. The implication is that FCC, as observed in the nuclear corpus, is specific to impulsive, near-isotropic sources with stable coda-to-main-phase amplitude ratios.

8 Particle Collision Domain: CERN CMS Open Data

As a cross-domain admissibility test in a physically unrelated setting, we evaluate structural ladders constructed from CMS Open Data: 104 $H \to ZZ \to 4\ell$ (2e2mu channel) collision events from the 2012 LHC run [16]. Three ladder representations are evaluated: the sorted invariant-mass gaps ($n = 103$), the sorted invariant-mass trajectory ($n = 104$), and an extended trajectory including auxiliary reconstruction information ($n = 207$). All three produce FULL percolation with GR = 1.000 (Table 8).

Table 8: STRUC-PERC-I v2.4.0 results for CMS $H \to 4\ell$ collision data.

Ladder representation	n	Verdict	GR	κ_{conn}	TD
Invariant-mass gaps	103	FULL	1.000	2.00	0.427
Invariant-mass trajectory	104	FULL	1.000	7.13	0.430
Extended trajectory	207	FULL	1.000	85.05	0.526

The connectivity threshold κ_{conn} scales with sample size and mass spread: 2.00 $\to$ 7.13 $\to$ 85.05 as n increases from 103 to 207. Tail dominance values (0.43–0.53) fall in the moderate range, between the non-seismic low-TD stations (IU.KIP: 0.193) and the supernova Δ-ladder (0.811). The CERN corpus is the only domain in which all representations, including the raw-state analog (invariant-mass gaps), produce FULL percolation without requiring a Δ-lift. This is consistent with the observation that invariant mass, as a Lorentz-invariant reconstruction quantity, already constitutes a transition-like observable: it is computed from the momentum differences among decay products rather than from absolute position in energy space.

9 Astrophysical Boundary Transport: Voyager Realizability Trajectories

The corpus assembled so far consists of short-duration explosive transitions: a supernova light curve spanning 80 days, seismic waveforms lasting minutes to hours, nuclear explosion recordings of seconds to tens of seconds, and particle collision events. A fundamentally different test of the Margin Collapse Hypothesis is provided by systems that evolve continuously over years while approaching and traversing a physical boundary. The Voyager 1 and Voyager 2 spacecraft supply exactly this: multi-year astrophysical trajectories through heliospheric plasma and magnetic field, culminating in the crossing of the heliopause—the boundary between the solar wind and the interstellar medium (ISM)—at distances exceeding 100 astronomical units from the Sun. Together they provide the first empirical test of UNNS realizability dynamics in a long-duration, nonterminal transport regime.

9.1 Voyager 1: Magnetic Field Trajectory Through the Heliopause

The Voyager 1 magnetic field corpus evaluates the 48-second $|B|$ (field magnitude) observable from the MAG primary dataset across 3,500 DLCP-compliant windows spanning 2011–2017, covering the pre-crossing heliosheath (2011), the heliopause crossing epoch (August 2012), and the post-crossing ISM phase (2013–2017). Instrument: STRUC-PERC-I v2.5.0; window width $\Delta = 1{,}024$ samples, stride 256. Table 9 presents the annual structural statistics.

Table 9: Voyager 1 $|B|$ structural trajectory: annual STRUC-PERC-I statistics (3,500 evaluations, 500 windows/epoch). GR: mean giant ratio; TD: mean tail dominance; κ_{conn}: mean connectivity threshold. Heliopause crossing: 25 August 2012.

Year	Phase	FULL	GIANT	TAIL	HARD	κ_{conn} mean	TD mean	GR mean
2011	Pre-crossing	463	26	10	1	18,187	0.781	0.9995
2012	Crossing	474	16	10	0	14,686	0.776	0.9997
2013	ISM	500	0	0	0	31,057	0.947	1.0000
2014	ISM	495	4	1	0	28,748	0.938	0.9999
2015	ISM	489	5	6	0	27,282	0.936	0.9998
2016	ISM	488	10	2	0	35,806	0.932	0.9998
2017	ISM	500	0	0	0	35,985	0.946	1.0000

9.1.1 Persistent Coherence: 97.4% FULL Dominance

Across 3,500 windows, 3,409 (97.4%) classify as FULL percolation with GR ≈ 1.000. This is the highest sustained FULL fraction of any UNNS corpus evaluated to date, exceeding even the Voyager 2 plasma corpus (96.0%). The single HARD window is an isolated 2011 anomaly (Theorem-1 active); no HARD outcomes appear in any subsequent epoch. The mean giant ratio remains between 0.9995 and 1.0000 throughout all seven years.

This constitutes a direct empirical realization of the Margin Collapse Hypothesis operating in the persistence regime: $m(L_t)$ decreases toward the heliopause crossing but never reaches zero, and the giant component is maintained throughout the full boundary transit.

9.1.2 Boundary-Adjacent Clustering: Excursion Concentration in 2011–2012

Of the 61 GIANT excursions in the corpus, 42 (69%) fall in the 2011–2012 pre-crossing and crossing epochs. The 2013 and 2017 ISM epochs are 100% FULL with zero excursions. This temporal clustering—boundary-adjacent classes concentrated near the physical boundary crossing—is a direct structural signature of the margin approaching 0^+ as the spacecraft traverses the heliopause. The pattern is consistent with the Forced Coherent Collapse regime: elevated excursion density corresponds to reduced margin, while GR remains near unity throughout.

9.1.3 κ_{conn}-Trajectory Restructuring at the Heliopause

The structural boundary estimator $t^* = 2012$ is identified as the annual κ_{conn} minimum, stable across all three tested window scales (Table 10).

After crossing, κ_{conn} jumps by a factor of 1.6–2.4× (scale-dependent), reflecting the structural restructuring of the magnetic field into the ISM regime. Simultaneously, mean

Table 10: Multi-scale robustness of the structural boundary estimator $t^* = 2012$. Post/crossing ratio: mean κ_{conn} over 2013–2017 divided by the 2012 minimum. All three scales unanimously identify 2012 as the κ_{conn} minimum, confirming the result is not an artifact of the baseline window size.

Scale	t^*	$\kappa_{\text{conn}}^{\text{min}}$ (2012)	$\kappa_{\text{conn}}^{\text{post}}$ (mean)	Post/crossing ratio
W512/S128	2012	5,872	13,984	2.38×
W1024/S256	2012	14,686	31,776	2.16×
W2048/S512	2012	47,562	78,113	1.64×

tail dominance increases from TD ≈ 0.78 (crossing) to TD ≈ 0.94 (ISM phase): the post-crossing ISM ladder is structurally heavier-tailed than the heliosheath, with κ_{conn} elevated but GR simultaneously rising to 1.0000 in 2013 and 2017. This is a post-crossing FCC-to-FULL stabilization: the boundary-adjacent margin minimum is followed by structural recovery into a high-coherence ISM state.

Observation 6 (Nonterminal Boundary Transport)**.** The Voyager 1 magnetic-field corpus demonstrates a complete boundary transit without global structural fragmentation: 3,409/3,500 windows remain FULL throughout heliosheath, crossing, and ISM phases; boundary-adjacent excursions are localized to 2011–2012 (GR ≥ 0.975 throughout); and the structural boundary estimator $t^* = 2012$ is stable across a 4× variation in window scale. This is *nonterminal boundary transport*: the system approaches the low-margin frontier, crosses a physical boundary, and recovers to a higher-κ_{conn} ISM state without ever triggering persistent HARD fragmentation.

9.2 Voyager 2: Observable-Dependent Realizability

The Voyager 2 heliosheath plasma corpus evaluates four observables (bulk velocity V, temperature T, thermal speed w, and number density ρ) across 628 STRUC-PERC-I v2.4.0 evaluations spanning 12 annual epochs (2007–2018). The corpus reveals a near-complete class separation by observable type, constituting the most direct empirical demonstration of *observable-dependent realizability* in the UNNS corpus to date.

Table 11: Voyager 2 heliosheath plasma: class distribution by observable (628 total evaluations, 2007–2018). The density observable returns ≈ 57 unique values per 1,024-sample window due to PLS fitting resolution limits, producing systematic HARD fragmentation unrelated to physical plasma structure.

Observable	FULL	HARD	Other	Total	Character
Velocity V	147	1	10	158	FULL dominant (93.0%)
Temperature T	153	0	4	157	FULL dominant (97.5%)
Thermal speed w	148	0	8	156	FULL dominant (94.9%)
Density ρ	2	155	0	157	HARD dominant (98.7%)

Velocity, temperature, and thermal speed are overwhelmingly FULL-class (93.0–97.5%). Density is 98.7% HARD, with 155 Theorem-1 activations. This separation is structural, not physical: the PLS fitting resolution in the outer heliosphere produces approximately 57 unique values per 1,024-sample window (a degeneracy ratio of ≈ 5.6%), independent of

heliocentric position or epoch. The density channel is a direct instance of Representation-Induced Structural Collapse driven by *measurement resolution* rather than propagation geometry.

The kinematic and thermal channels independently confirm the Voyager 1 findings: sustained FULL dominance across 11 years, boundary-adjacent excursions (22 TAIL/GIANT windows) concentrated near the pre-heliopause epoch (2017–2018), and multi-variable κ_{conn} convergence as the spacecraft approaches the heliopause.

9.3 Voyager as a Test of the Margin Collapse Hypothesis

The Voyager corpus provides three results not available from the explosive-transition domains of Sections 3–8:

1. FCC in long-duration transport. Explosive systems (supernovae, nuclear explosions, seismic ruptures) exhibit FCC-like structure over durations of seconds to days. Voyager 1 demonstrates FCC-adjacent behavior sustained over years of continuous magnetized plasma transport. The boundary-adjacent excursions of 2011–2012 are not abrupt collapses but gradual margin reductions under sustained heliospheric forcing. This extends the FCC regime beyond impulsive events into the class of *continuous boundary-approach dynamics*.

2. Nonterminal boundary transport vs. forced collapse. Explosive systems are terminal: the supernova light curve ends, the nuclear explosion record terminates. Voyager 1 is nonterminal: it crosses the heliopause and continues to produce structurally coherent $|B|$ ladders in the ISM. The post-crossing κ_{conn} recovery (factor 1.6–2.4× above the crossing minimum) and 100% FULL years in 2013 and 2017 demonstrate that the realizability trajectory recovers after boundary transit—the system exits FCC-adjacent conditions upon entering the ISM. This is the structural signature of a boundary crossing rather than a terminal fragmentation event, and it could not have been demonstrated without a spacecraft that actually traverses the boundary.

3. Observable-dependence as a second representation axis. The Voyager 2 density channel adds a new dimension to Representation-Induced Structural Collapse: beyond propagation-distance effects (Nevada) and raw vs. Δ-layer effects (SN Ia), RISC can also arise from *measurement resolution limits* that discretize the observable into a ladder too sparse to support giant-component connectivity. The three RISC mechanisms now empirically documented are: (a) absolute-scale embedding gap dominance (SN Ia raw magnitude); (b) propagation-distance attenuation (Nevada teleseismic); (c) measurement-resolution discretization (Voyager 2 density). All three produce Theorem-1 activation in the affected observable while the underlying physical system remains structurally coherent in alternative representations.

Observation 7 (Voyager and the Margin Collapse Hypothesis)**.** The Voyager corpora are consistent with the Margin Collapse Hypothesis operating in the continuous-transport regime: $m(L_t)$ decreases as Voyager 1 approaches the heliopause (boundary-adjacent GIANT/TAIL excursions cluster in 2011–2012; κ_{conn} reaches its minimum in the crossing year), crosses the boundary without reaching $m = 0$ (no persistent HARD), and recovers

to a higher-margin ISM state post-crossing. This is the first empirical trajectory in the UNNS corpus that enters, traverses, and exits a boundary region in realizability space while maintaining admissibility throughout.

10 κ-Evolution and Local Structural Fracture

10.1 Sliding-Window Analysis

To probe the dynamic evolution of structural tension in the supernova energy ladder, we apply a sliding-window analysis using $N_w = 30$ windows of size $w = 7$ over the energy ladder L^{energy} (ZTF20acobvxk, $n = 37$ elements, $E_i = 10^{-0.4\,m_i}$). For each window W_j ($j = 0, \ldots, 29$), the local tension $\tau_{W_j}(L)$ is computed via (3). Figure 5 displays the resulting tension profile.

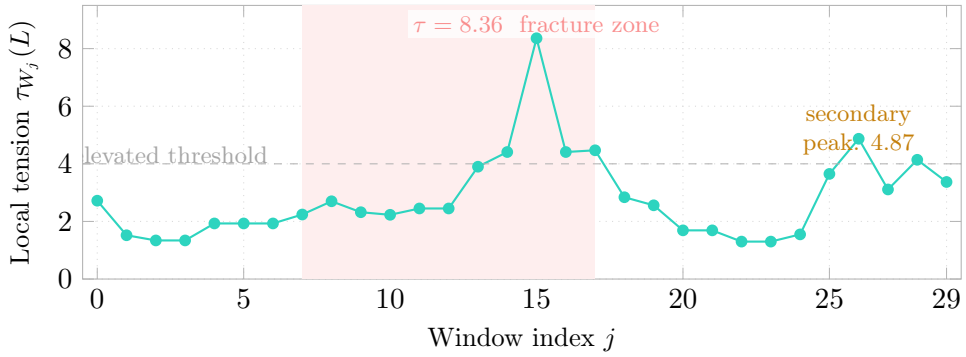

Figure 5: Sliding-window structural tension $\tau_{W_j}(L)$ over 30 windows of size $w = 7$ applied to the ZTF20acobvxk energy ladder ($n = 37$, $E = 10^{-0.4m}$). The shaded region (windows 7–17) marks the fracture zone, peaking at $\tau_w = 8.36$ (window 15). A secondary elevated-tension region appears at windows 25–28 ($m \approx 3.1$–4.9), corresponding to the late-decline tail of the light curve. Tension values outside these regions remain in the range 1.3–2.8×, indicating stable low-tension structure.

10.2 Fracture-Point Identification and Removal

Global percolation analysis of the full energy ladder yields HARD-fragmentation (GR = 0.944, $\kappa_{\text{plateau}} = 2$, Theorem-1 active). Fracture analysis identifies the dominant outlier gap at index 9 of the 37-element ladder, with gap magnitude $\delta_9 = 1.865 \times 10^{-8}$ versus median gap $\bar{\delta} = 6.1 \times 10^{-10}$ (ratio $\approx 30.6\times$). Removal of this single element reduces the ladder to $n = 36$ elements and yields FULL percolation: GR = 1.000, $\kappa_{\text{conn}} = 0.750$, Theorem-1 not activated.

The recovery from HARD to FULL upon removal of a single element demonstrates that the global HARD-fragmentation verdict of the full energy ladder is driven by one localized outlier gap, not by distributed structural collapse. This is analogous to the SN Ia raw-magnitude finding: a single dominant gap in the absolute-scale embedding disrupts global connectivity, while the underlying structural texture of the system is otherwise admissible.

Observation 8 (Local fracture, global recovery)**.** In the ZTF20acobvxk energy ladder, removal of a single fracture element (gap ratio 30.6× above the median) restores global

FULL percolation. The HARD-fragmentation verdict of the full ladder is localized to one structural discontinuity and does not reflect distributed collapse.

11 Cross-Domain Synthesis

11.1 The Δ-Representation as a Structural Stabilizer

Table 12 summarizes the central empirical result of this manuscript: the verdict transformation under the Δ-lifting across all five tested domains.

Table 12: Cross-domain structural summary. Raw state: verdict from the sorted raw observable. Δ-state: verdict from the transition-difference representation. For domains where the raw observable already constitutes a transition quantity (CERN), both columns agree.

Domain	Raw-state verdict	Δ-state verdict	Structural character
SN Ia (ZTF20acobvxk)	HARD (Th. 1, GR = 0.952)	FULL (GR = 1.00, κ_{conn} = 141, TD = 0.81)	Admissible heavy-tail
Seismic (May 2026)	—	FULL/GIANT (GR $\geq$ 0.997)	Structurally stable
Nevada earthquake	mixed (station-dep.)	FULL→HARD; propagation-induced	Representation-distance effect
NK explosion corpus	—	GIANT/TAIL; zero HARD; FCC at proximal stations	Forced Coherent Collapse (yield trajectory)
CERN $H \to 4\ell$	FULL (GR = 1.00)	FULL (GR = 1.00)	Transition-native rep.
V1 $\lvert B\rvert$ heliosheath	—	FULL (97.4%); FCC-adj. 2011–12	Nonterminal boundary transport
V2 plasma (V,T,w)	—	FULL dominant; pre-HP excursions	Continuous boundary approach
V2 density ρ	HARD (98.7%, RISC)	HARD (resolution-induced)	Observable-resolution RISC

Four synthesis statements follow from the corpus:

A. Transition-space organization is more structurally stable. In every domain where a raw-state and a Δ-state comparison is available, the Δ-layer produces an equal or higher realizability class. The sole exception—the Nevada HARD-class at IU.HRV—is attributable to the propagation-distance embedding rather than to any failure of the Δ-layer itself. Across 48 ladder evaluations, zero cases are found in which the Δ-representation degrades a raw-state FULL verdict to a lower class.

B. Coherent persistence under heavy-tail concentration. The real structural discovery is not that Δ-layer representations are heavy-tailed—many physical signals are—but that *admissible giant-component connectivity persists under extreme tail concentration.* Tail dominance values in the Δ-layer span 0.43–0.81 for the supernova, seismic, and CERN domains; the NK corpus extends this to near-saturation (TD → 1.0). In every case, GR

remains at or above 0.97. The novelty is the preserved coherence, not the tail structure per se.

C. Extreme transition systems preserve connectivity more robustly than naïve expectation; source geometry matters. Despite the destructive energetics involved, the 29 station-event nuclear explosion evaluations produce zero Theorem-1 activations. The most extreme system in the corpus (IC.MDJ, Event 3, TD = 0.997) maintains GR = 0.975. Structural connectivity in transition space is demonstrably robust even under conditions that would be considered physically extreme. Crucially, the FCC regime has spatial structure: proximity to the source organizes stations along an increasing-TD/stable-GR trajectory (Sections 6.8.2–6.8.3). This behavior is governed by the Unified Tail Dominance Scaling Law (Proposition 9), which extends source-strength and distance-attenuation scaling into a single cross-domain transport law: $\mathrm{TD}(S,d) = \beta_0\phi(S)\psi(d)/(1+\beta_0\phi(S)\psi(d))$. The law provides the same functional form for nuclear explosions, earthquakes, and supernova light curves—three systems with no common microscopic physics—and produces falsifiable scaling predictions in each domain (negative $\partial\mathrm{TD}/\partial d$; positive $\partial\mathrm{TD}/\partial S$; saturation to $\mathrm{TD} \to 1$ at proximal stations). This moves the FCC description from static taxonomy into *realizability transport*: directional movement in the $(\mathrm{TD}, \mathrm{GR})$ phase plane governed by a propagation law.

D. Observed fragmentation may be representational. In the SN Ia case, the fracture-removal analysis, and the Nevada station-distance gradient, the data consistently indicate that HARD-fragmentation arises from the structure of the observation rather than from the structure of the system. No domain in this corpus exhibits a case where the Δ-layer itself produces HARD-fragmentation from a physically smooth system.

E. Limits of the Δ-lifting: explicit negative result. The Δ-lifting does not universally recover FULL percolation, and this manuscript does not claim otherwise. Three documented instances resist full recovery. First, the Nevada station IU.HRV produces HARD fragmentation in the ΔA ladder: here the Δ-layer itself fails to recover FULL due to a propagation-geometry embedding that collapses ladder size to $n = 217$ with a dominant outlier gap—Representation-Induced Structural Collapse is not eliminated by differencing when the observational deformation is severe enough. Second, the NK corpus shows no FULL-class verdicts at any station-event pair: all ΔA ladders remain in TAIL or GIANT class. The Δ-lifting stabilizes connectivity ($\mathrm{GR} \geq 0.971$) but cannot fully remove the structural imprint of the extreme amplitude events on the gap distribution. Third, the ZTF energy ladder post-fracture yields FULL only after explicit outlier removal; the Δ-lifting alone on the energy representation does not suffice without the fracture step. These cases delimit the boundary of the Δ-stabilization effect: it reliably prevents HARD outcomes in physically smooth systems, but propagation-induced signal degradation and extreme impulsive forcing can maintain sub-FULL structures even in the transition representation.

11.2 Central Proposition

The findings of Sections 3–10 are unified by the following corpus-scoped proposition:

Proposition 10 (Transition-Space Structural Persistence)**.** *For the tested corpus, Δ-representations systematically preserve or improve realizability class relative to raw-state representations, maintaining giant-component connectivity (*GR ≥ 0.97*) while concentrating gap mass into heavy-tail structure (*TD > 0.4*). Raw-state* HARD*-fragmentation is consistently recoverable by the Δ-lifting in cases where the source system is physically smooth and the observational embedding is not severely deformed.*

Remark 2 (Corpus scope)**.** Proposition 10 is empirical and corpus-scoped. It holds for the five tested domains (ZTF20acobvxk, IU/IC seismic network, NK explosion dataset, CMS 2012) and is not asserted universally. The proposition is falsifiable: a single domain in which the Δ-layer degrades a raw-state FULL verdict to HARD without a propagation-geometry explanation would constitute a counterexample. No such case has been found in the present corpus.

11.3 Unified Admissibility Atlas

Figure 6 plots all evaluated systems in the two-dimensional structural space of tail dominance TD versus giant ratio GR. The four quadrants delineate the structural regimes.

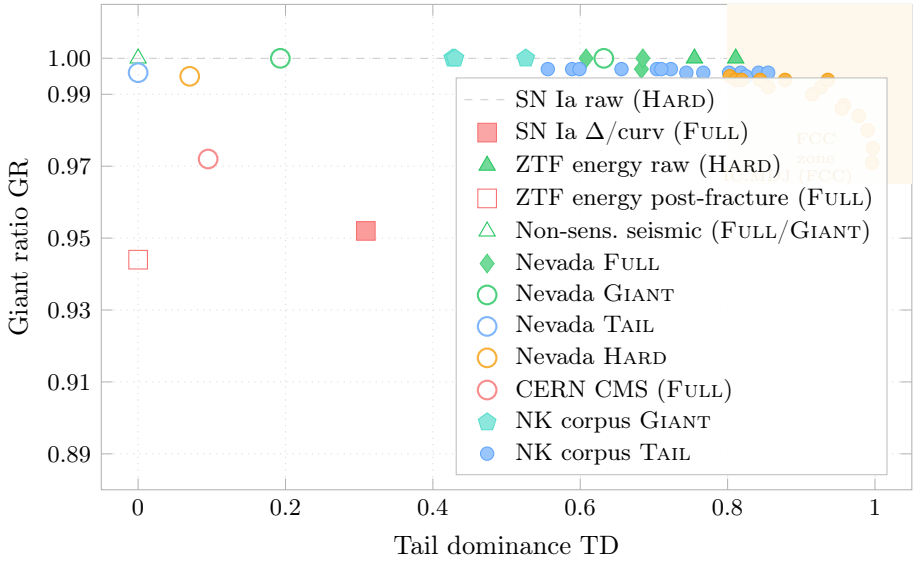

Figure 6: Unified admissibility atlas: all evaluated systems in the (TD, GR) structural plane. Raw-state ladders producing HARD fragmentation appear in the lower-left region (GR < 0.96, low TD). The Δ-layer consistently lifts systems into the upper half of the plot (GR > 0.97). The nuclear explosion corpus (filled circles) occupies the right portion of the upper band, reaching the Forced Coherent Collapse zone (shaded, upper right: TD > 0.80, GR > 0.97). CERN evaluations (pentagons) cluster at moderate TD, GR $= 1.00$.

12 Theoretical Implications

12.1 Transition-Space Observability

The corpus results indicate that the Δ-representation yields more stable realizability classifications than raw-state coordinates, and reduces embedding-induced discontinuities that

would otherwise activate Theorem-1. Within the Dual Observability framework [3], the two structural observables ($\bar{\rho}$ from STRUC-I and $\mathcal{C}$, κ_{conn} from STRUC-PERC-I) constitute independent coordinates of $\mathcal{M}_{\text{adm}}$. The Δ-transformation does not alter admissibility ($\bar{\rho}$) but systematically shifts realizability class ($\mathcal{C}$) toward FULL or GIANT. The operational consequence is that raw-state embeddings yield realizability classes that are systematically lower than those obtained from transition-space coordinates, without corresponding changes in the admissibility score. Transition representations therefore probe the connectivity structure of the underlying process more directly than absolute-scale embeddings.

12.2 Structural Persistence Under Extreme Transitions

The nuclear explosion corpus provides the most direct evidence that connectivity is preserved more robustly under extreme transitions than raw-state representations would suggest. Across 29 evaluations with TD reaching 0.997, giant-component connectivity remains above GR = 0.971 throughout. The Voyager 1 corpus provides the complementary evidence from a long-duration transport regime: 97.4% FULL dominance across 3,500 windows spanning a seven-year heliopause approach and crossing, with boundary-adjacent excursions concentrated near 2011–2012 and GR never falling below 0.975 throughout (Observation 6). Together, the shared pattern across astrophysical and geophysical corpora is that transition-space ladders concentrate gap mass into the outlier tail under strong forcing while the background bulk maintains sufficient connectivity density to support a giant component. The Voyager corpus additionally demonstrates that this connectivity is maintained across a physical boundary crossing and that the system recovers to a higher-margin state post-crossing—a trajectory unavailable in terminal explosive systems.

12.3 Admissibility Under Stress

The phase-mapping study [4] established Bounded Structural Rigidity: the realizability class $\mathcal{C}(L)$ is invariant within a finite stability region Ω_L around the physical parameter point, for every tested admissible ladder. The present corpus adds a complementary result along a different axis: the transition-space representation yields a higher realizability class than the raw-state embedding for the same physical process, and that improvement is maintained even under extreme deformations (high TD, near-FCC conditions). The Δ-lifting therefore acts as a representational stabilizer: it maps the system into a higher-connectivity region of $\mathcal{M}_{\text{adm}}$ that is more robust to large-scale gap fluctuations than the raw-state image.

12.4 Representation-Induced Collapse

The Nevada earthquake corpus and the SN Ia raw-ladder finding jointly establish that observational embedding can produce genuine Theorem-1 activation in systems whose Δ-layer counterparts remain FULL or GIANT. The distinction to maintain is that Representation-Induced Structural Collapse generates valid results for the observable it characterizes: at IU.HRV, the ΔA ladder satisfies Theorem-1 conditions as constructed, and that verdict accurately describes the structural properties of the teleseismic ΔA sequence at that station. What RISC identifies is that the verdict reflects the propagation embedding rather

than the source dynamics. Operationally, this means that single-station structural assessments of distant seismic sources should not be interpreted as source-characterizing without a multi-station comparison to separate source from path effects.

12.5 Dynamic Structural Coherence and Open Extensions

The sliding-window analysis of Section 10 demonstrates that structural tension is heterogeneously distributed over the ladder: the energy ladder of ZTF20acobvxk exhibits stable low tension ($\tau_w \approx 1.3$–2.7) over most of its range, elevated tension in a localized fracture zone (windows 7–17, peak $\tau_w = 8.36$), and moderate secondary tension in the late-decline tail. This pattern is directly consistent with the Margin Collapse Hypothesis (Section 1): the system traverses a local margin minimum at the fracture point (corresponding to $m(L_t) \to 0^+$ locally) while remaining in the admissible interior globally. The fracture removal that restores FULL percolation (Section 10.2) is structurally the operation of lifting $m(L_t)$ back above zero by excising the critical gap that drives the margin to its minimum. A complete dynamic treatment would compute formal $m(L_t)$ margin trajectories using Definition 1 and the proxy of (5) for both the supernova and seismic corpora, and compare their temporal profiles to the proposed dynamical model (6). This would directly test whether margin-collapse trajectories are shared across domains under transition stress, and would provide the first empirical measurement of the mean-field exponents proposed in Section 2.5. It is the primary open quantitative extension of the present work.

13 Conclusion

We have presented a cross-domain empirical analysis of structural admissibility spanning six physically distinct extreme-transition and boundary-transport systems, evaluated via STRUC-PERC-I v2.4.0–2.5.0 across 48 ladder evaluations, 29 station-event nuclear explosion recordings, and 4,128 Voyager magnetic-field and plasma window evaluations.

The central empirical findings are:

1. **Δ-space admissibility.** In all tested cases where the source system is physically smooth and the observational embedding is not severely propagation-deformed, the Δ-representation recovers FULL or GIANT-class percolation. Severe propagation embedding can still produce HARD fragmentation, as demonstrated by IU.HRV (Nevada earthquake, teleseismic distance). The Δ-lifting is a structural stabilizer, not an unconditional recovery guarantee.

2. **Hidden structural coherence.** Systems that appear fragmented in raw-state representations (SN Ia raw magnitude, ZTF energy ladder) exhibit full percolation in the Δ-representation. The fragmentation is representational rather than physical in both documented cases.

3. **Forced Coherent Collapse.** The nuclear explosion corpus introduces a structural regime in which near-total tail domination (TD $\to 1$) co-exists with preserved giant connectivity (GR > 0.97) and the complete absence of hard fragmentation (Definition 3). Six mathematical properties of FCC are derived in Section 6.6, including

the tail saturation bound, connectivity margin preservation, boundary characterization with HARD fragmentation, and the yield-intensity scaling law ($d\,\mathrm{TD}/dY > 0$, $d\,\mathrm{GR}/dY \approx 0$, Propositions 2–7).

4. **Limits of the Δ-lifting.** The Δ-representation does not universally recover FULL percolation. Three documented exceptions constrain the result: severe propagation-geometry deformation (IU.HRV, Nevada); impulsive-forcing-dominated gap distributions (NK corpus: no FULL outcomes); and energy-scale representations requiring explicit fracture removal before the Δ-step (ZTF energy ladder). These cases delimit the boundary of the Δ-stabilization effect.

5. **Central proposition.** The Transition-Space Structural Persistence Proposition (Proposition 10) states: for the tested corpus, Δ-representations systematically yield equal or higher realizability class than raw-state representations while maintaining $\mathrm{GR} \geq 0.97$. This is an empirical, corpus-scoped, falsifiable statement. No counterexample has been found in the present data.

6. **Unified Tail Dominance Scaling Law.** The Unified Scaling Law (Proposition 9) provides the first cross-domain transport law of FCC/Tail realizability: $\mathrm{TD}(S,d) = \beta_0\phi(S)\psi(d)/(1+\beta_0\phi(S)\psi(d))$, with positive source-strength dependence and negative distance/redshift dependence. This extends the FCC framework from static classification into realizability transport: directional movement in the $(\mathrm{TD}, \mathrm{GR})$ phase plane governed by a propagation law that admits the same functional form across nuclear explosions, natural earthquakes, and supernova light curves. Three falsifiable predictions follow: negative TD–z correlation in larger ZTF supernova samples; negative TD–distance correlation in regional earthquake networks; and $\mathrm{TD} \to 1$ saturation at proximal nuclear explosion stations.

7. **Representation-Induced Structural Collapse.** The Nevada earthquake corpus demonstrates that structural verdict can degrade from FULL to HARD under changes in observational geometry (propagation distance) without any change in the physical source. This establishes Representation-Induced Structural Collapse as a well-defined observational phenomenon requiring careful interpretation of single-station assessments.

8. **Cross-domain convergence.** Despite spanning energy scales from seismic (10^{10}–10^{17} J) to astrophysical (10^{43}–10^{44} J), and timescales from seconds (nuclear explosions) to years (Voyager), all tested domains produce structurally similar Δ-layer signatures: heavy-tail ($\mathrm{TD} > 0.4$), high giant ratio ($\mathrm{GR} > 0.97$), and coherent global connectivity.

9. **Nonterminal boundary transport (Voyager).** The Voyager 1 magnetic-field corpus (3,500 window evaluations, 2011–2017) demonstrates that a system can approach a physical boundary ($m(L_t) \to 0^+$, boundary-adjacent excursions in 2011–2012), traverse it (heliopause crossing, August 2012), and recover to a higher-coherence state (κ_{conn} factor 1.6–2.4× higher in ISM phase) without triggering persistent HARD fragmentation—97.4% FULL throughout. This extends FCC-adjacent dynamics beyond impulsive events into long-duration continuous-transport systems. The Voy-

ager 2 density channel simultaneously demonstrates a third mechanism of Representation-Induced Structural Collapse: measurement-resolution discretization, distinct from propagation-distance attenuation (Nevada) and absolute-scale embedding (SN Ia).

All findings are scoped to the tested corpus. No claim of universality beyond the datasets evaluated here is made. The hypothesis that transition-space organization yields more stable realizability structure than raw-state organization within the tested corpus is an empirical observation supported by the present data, presented here as a working principle for future investigation.

The present manuscript connects directly to the broader UNNS research program along several lines. The Bounded Structural Rigidity result [4] established that realizability class is invariant within a finite stability region around each physical parameter point; the Margin Collapse Hypothesis extends this into the dynamical regime, characterizing how that region shrinks under forcing. The Unified Scaling Law (Proposition 9) provides the first cross-domain transport law linking the phase-landscape geometry of $\mathcal{M}_{\text{adm}}$ to observable propagation parameters. The Dual Observability framework [3] supplies the two-coordinate system $(\bar{\rho}, \mathcal{C})$ within which the Δ-representation's effect on realizability class can be formally quantified without altering admissibility. The trajectory program [10, 9] is extended here from the Voyager 2 plasma corpus to Voyager 1 magnetic field and into a new regime class (nonterminal boundary transport), while the Voyager results directly support the margin-trajectory interpretation of κ_{conn} minimization at the heliopause. Together, these connections position the Margin Collapse Hypothesis as an organizing principle that links the static realizability geometry of earlier UNNS work to the dynamical structural evolution observed under extreme physical forcing.

Across all tested domains, transition-space representations repeatedly recover coherent admissible organization even when raw observational structure appears fragmented. The results suggest that structural continuity in physical systems may reside more fundamentally in transition geometry than in state geometry itself.

Acknowledgements

This work is part of the UNNS Substrate Research Program. All data used are from public repositories. Seismic data are courtesy of the IRIS/FDSN network. Nuclear explosion seismic data are from the IRIS Data Management Center special event archive for the 2013 North Korea nuclear test (https://ds.iris.edu/ds/nodes/dmc/specialevents/2013/02/12/north-korea-nuclear-explosion/) [15]. CMS collision data are from the CERN Open Data Portal, record 5200 (https://opendata.cern.ch/record/5200). Photometric data for ZTF20acobvxk are from the Zwicky Transient Facility public archive. Voyager 1 MAG data are from NASA CDAWeb (dataset: Voyager1_MAG_pri_48s). Voyager 2 plasma data are from NASA CDAWeb (dataset: VOYAGER2_PLS_HIRES_PLASMA_DATA_HSH).

References

[1] UNNS Substrate Research Program. The Universal Structural Law: Admissibility Bounds on Ordering Instability. An Empirical Investigation Across 3,073 Physical Ladders Spanning Thirteen Physical Domains. *UNNS Working Manuscript*, 2026.

[2] UNNS Substrate Research Program. The Percolative Realizability Principle: Realizability Structure of Admissible Configurations and the Revised Necessary Direction. *UNNS Working Manuscript*, 2026.

[3] UNNS Substrate Research Program. Structural Realizability and Dual Observability in the Admissibility Manifold: A Second Structural Layer Between Admissibility and Dynamics. *UNNS Working Manuscript*, 2026.

[4] UNNS Substrate Research Program. Phase Mapping of Structural Regimes in the UNNS Substrate: Bounded Structural Rigidity and Representation-Driven Structure. *UNNS Working Manuscript*, April 2026.

[5] UNNS Collective. Structural Persistence Across Four Empirical Domains: A Unified Cross-Domain Certification of the UNNS Admissibility Geometry Framework. *UNNS Research Program*, Version 1.0, March 2026.

[6] UNNS Collective. Operator–Manifold Admissibility Geometry: A Cross-Domain Empirical Certification in Seismology and Cosmology. Independent Research Group, Version 1.0, March 2026.

[7] UNNS Substrate Research Program. Structural Invariance and Domain-Selective Response Under Fundamental Constant Deformation: An Empirical Investigation Across Four Fundamental Constants and Seven Physical Domains. *UNNS Working Manuscript*, 2026.

[8] UNNS Substrate Research Program. Foundations of the UNNS Substrate: From Universal Admissibility to Structural Regime Theory. *UNNS Foundation Document*, 2026.

[9] UNNS Substrate Research Program. Structural Trajectories in Realizability Space: Voyager 2 Plasma as a Time-Resolved Test of the UNNS Substrate. *UNNS Working Manuscript*, 2026.

[10] UNNS Substrate Research Programme. Structural Phase Transitions Along Physical Trajectories: Voyager Data as a Dynamic Realization of Realizability Geometry. *UNNS Working Manuscript*, 2026.

[11] UNNS Substrate Research Program. Local Geometry of Realizability Boundaries in the UNNS Substrate. *UNNS Working Manuscript*, 2026.

[12] UNNS Substrate Research Program. Admissibility Constraints Across Physical and Biological Systems: An Empirical Extension of the Universal Structural Law. *UNNS Working Manuscript*, 2026.

[13] UNNS Substrate Research Program. Structural Response to Fundamental Constant Deformations: Operator Algebra, Phase Transitions, and Invariance Classes in the UNNS Substrate. *UNNS Working Manuscript*, 2026.

[14] UNNS Substrate Research Program. Emergent Dimensionality in the UNNS Substrate: Connectivity Margin as the Generator of Observable Degrees of Freedom. *UNNS Working Manuscript*, April 2026.

[15] IRIS Data Management Center. North Korea Nuclear Explosion Special Event, 12 February 2013: Seismic Data and Relocation Exercise. Incorporated Research Institutions for Seismology (IRIS), 2013. https://ds.iris.edu/ds/nodes/dmc/specialevents/2013/02/12/north-korea-nuclear-explosion/

[16] CMS Collaboration. CMS Open Data: $H \to ZZ \to 2e2\mu$ candidate events, 2012 dataset (Record 5200). CERN Open Data Portal, 2016. https://opendata.cern.ch/record/5200